A Novel Constrained Car-Following Control System for Autonomous Vehicles with Only Relative Distance and Angle Measurements

Khoshnam Shojaei and Allahyar Montazeri

***Abstract*—This paper proposes a novel coordinated car-following controller for two connected Ackermann steering vehicles subjected to actuator saturation, model uncertainties, limited filed-of-view, limited sensing and communication ranges, without velocity measurements, without collision between vehicles, and with path curvature compensation. To comply with the controller design, relative constrained distance and angle between vehicles are transformed into an efficient Euler-Lagrange formulation in terms of unconstrained errors. Then, two new sets of nonlinear filtered error variables are devised to propose a novel saturated proportional-integral-derivative observer-based control scheme which takes the advantages of the amplitude-limited PID control structure. The unknown model parameters and external disturbances are compensated via an operational combination of an adaptive robust control (ARC) scheme and a neural network (NN). The controller stability is proved by Lyapunov's direct method. Comparative simulation results will show the main benefits of the proposed control system.**

***Index Terms*—Adaptive neural controller, autonomous vehicle, collision avoidance, path curvature, saturated PID control.**

I. Introduction

THE coordinated tracking control of connected autonomous vehicles is an interesting topic of researches in intelligent transportation in recent decades. This interest is growing fast due to many advantages of automated vehicles platooning such as reducing fuel consumption, reducing highway congestion, increasing road capacity and safety enhancement. In the coordinated control of connected vehicles with a set of following vehicles and a leader one, each vehicle receives required information from its neighbours via wireless communication and the main control objective is to guarantee a safe distance and spacing between two consecutive vehicles while ensuring some pre-assigned constraints.

There exist many useful results on the motion control of autonomous vehicles in the literature [1–7]. Recently, a robust nonlinear controller has been presented for the lateral control of autonomous vehicles by using barrier Lyapunov function in [8]. A passivity-based path tracking controller was proposed for the autonomous vehicles in [9] by considering the yaw stability. A lateral and longitudinal dynamics control system has been addressed in [10] for autonomous vehicles based on multi-parameter joint estimation. In [11], a robust adaptive path-tracking controller was proposed for autonomous ground vehicles by considering backlash nonlinearity in the steering system. An event-triggered fixed-time controller has been presented for the planar vehicles platoon with distance constraints in [12]. A time-varying control-dependent barrier function method was used in [13] to design a tracking controller for autonomous ground vehicles. An adaptive constrained path following control system has been proposed for electric autonomous vehicles in [14]. An adaptive model predictive controller was presented for autonomous vehicles in [15]. In [16], a path tracking controller has been proposed for underactuated vehicles in the presence of matched and mismatched uncertainties. In [17], a cooperative constrained controller was proposed for autonomous vehicles without any collision with non-uniform input quantization via the backstepping design procedure. Very recently, some interesting results on the control of autonomous vehicles are presented in [18], [19], [20], [21], [22], [23] and [24]. However, there exist the following common drawbacks and shortcomings in the previous works: (i) most of the available results often rely on the proportional, or proportional-derivative (PD) feedback control schemes and there are few works that take the advantages of proportional-integral-derivative (PID) controller to simultaneously and efficiently tune the transient and steady-state characteristics of tracking errors [21], [25]; (ii) the previous controllers require the absolute $x - y$ positions of the vehicle from a global positioning system for outdoor applications; (iii) unfortunately, the majority of previous controllers in the recent literature focus on the backstepping design approach that experiences a design complexity; (iv) the most of the proposed controllers in the literature are not able to ensure the prescribed performance and their singularity is unavoidable in practice; (v) it is often assumed that the real onboard sensors are able to measure every possible value of posture variables and their limited sensing range and field-of-view are ignored in the previous works; (vi) the previous controllers suffer from unwanted deviations due to the path curvature during the turning of the vehicles on the corners; (vii) the most of proposed controllers absolutely require the measurements of linear and angular velocities for their implementations in practice; and (viii) the

Khoshnam Shojaei is with the Department of Electrical Engineering, Na.C., Islamic Azad University, Najafabad, Iran, and also with Digital Processing and Machine Vision Research Center, Na.C., Islamic Azad University, Najafabad, Iran (e-mail: khoshnam.shojaee@gmail.com).

A. Montazeri is with School of Engineering, Lancaster University, Gillow Avenue, Lancaster, England, LA14YW, e-mail: (a.montazeri@lancaster.ac.uk). The work is supported in part by the ASUNDER - Adaptable Semiautonomous Underwater Decommissioning Sample Retrieval Robot, EP/V027379/1, funded by EPSRC.

Manuscript received ***; revised ****.

adverse effects of the vehicle's actuator saturation due to the generation of large control signals from the controllers are neglected in the most of available works.

Based on the above mentioned deficiencies in the previous works, the *main motivation of this paper* is the proposing of a novel saturated nonlinear PID output-feedback controller (OFBC) for the cooperative car-following for an autonomous vehicle based on relative distance and angle measurements from the local onboard sensors with limited sensing range and field-of-view in the presence of the actuator saturation, model uncertainties, path curvature and in the absence of velocity signals while avoiding collisions and preserving a continuous connectivity. *Main novelties and contributions in this paper* are listed as follows with respect to the current literature [8]-[25]: (C1) By introducing new auxiliary filtered error variables, a saturated proportional-integral-derivative controller is heuristically proposed which reduces the amplitude of the generated control efforts by employing a class of saturation functions. The controller only depends on relative distance and angle measurements between vehicles. (C2) The controller prevents undesirable singularities due to an unwanted overshoot or undershoot during the transient response, avoids possible collisions between succeeding and preceding vehicles and preserves their continuous connectivity by utilizing the prescribed performance control (PPC) technique [26] which allows the designer to pre-assign maximum overshoot or undershoot, convergence speed and steady-state error for a safe car-following system. (C3) The proposed controller diminishes undesirable deviations of the preceding vehicle during the turning of the succeeding vehicle via compensating the path curvature by incorporating a correction angle in the definition of the relative angle error between vehicles. (C4) A novel nonlinear velocity observer is proposed to exclude linear and angular velocity sensors from the vehicle due to their inaccuracies in practice because of communication delays and noise contamination. The proposed observer is independent from the vehicle dynamics and prevent unwanted peaking. (C5) The danger of actuator saturation is reduced by restricting the amplitudes of tracking and observation errors in the controller and observer and by estimating the actuator saturation nonlinearity. (C6) Parametric uncertainties, external disturbances, unmodeled dynamics and neural network (NN) approximation errors are compensated by an operational combination of NN, adaptive and robust control schemes.

In the remaining sections, the following order is considered for the results in this paper. The problem formulation is described in Section II. Main results are given in Section III. Numerical computer simulation results are shown in Section IV and Section V concludes this paper finally.

II. PROBLEM STATEMENT

A. Notations

During the whole of this article, the operator $\| \bullet \|_F$ represents the Frobenius norm of an arbitrary matrix, $\| \bullet \|$ depicts the Euclidean norm, $tr\{\bullet\}$ displays the trace operator, $\mathbb{R}^+$ shows real positive number set, $\lambda_{min}\{\bullet\}$ and $\lambda_{max}\{\bullet\}$ respectively denote minimum and maximum values of an arbitrary matrix, $diag[\bullet]$ is a diagonal matrix, Proj$(\bullet)$ stands for the projection operator which is defined in [27], $\{a_i\}_{i=1}^n := \{a_1, a_2, \ldots, a_n\}$, $\mathcal{N}_f(x) := [n_{f1}(x), ..., n_{fn}(x)]^T$ and $\mathcal{S}_f(x) := [s_{f1}(x), ..., s_{fn}(x)]^T$ show vectors of nonlinear differentiable saturation functions which are defined later.

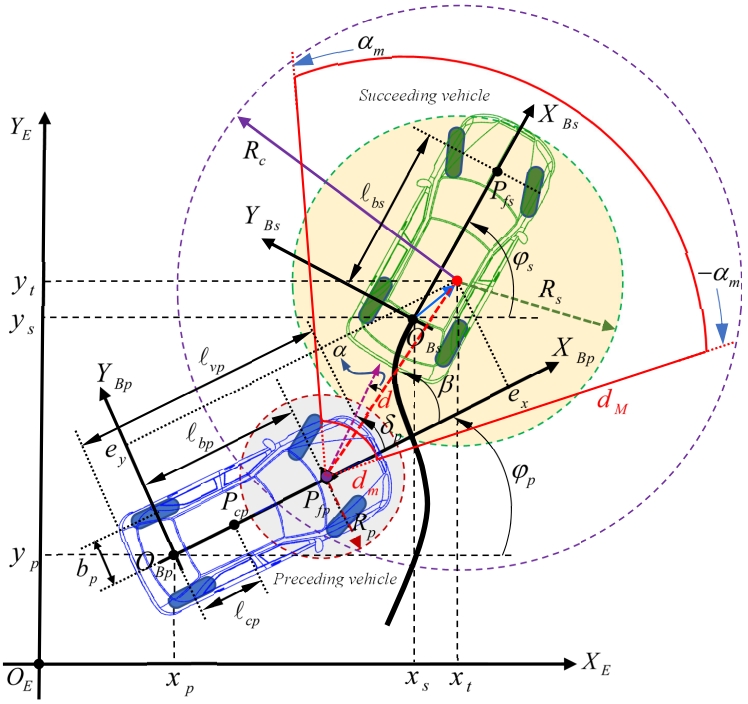

Fig. 1: The planar configuration of autonomous car tracking.

B. Autonomous Vehicle Model

Take into account the mathematical models of the autonomous vehicle with Ackermann steering as follows [25]:

$$\dot{q_j} = H(q_j)\nu_j, \forall j = p, s, \tag{1}$$

$$M_\nu(q_j)\dot{\nu}_j + C_\nu(q_j, \nu_j)\nu_j + D_\nu(q_j)\nu_j + \tau_{\nu d}(t) = B_\nu(q_j)\tau_{sj}, \tag{2}$$

where $q_j = [x_j, y_j, \varphi_j, \delta_j]^T$ denotes the vehicle posture in earth-fixed frame $\{O_E, X_E, Y_E\}$ based on Fig. 1, $\nu_j = [v_j, \omega_j]^T$ displays a vector of vehicle velocities such that ω_j and v_j respectively show angular and linear velocities of point O_{Bj}, $H(q_j) = [H_1(q_j), H_2(q_j)] \in \mathbb{R}^{4\times 2}$ with $H_1(q_j) = [cos(\varphi_j), sin(\varphi_j), 1/\ell_{bj} tan(\delta_j), 0]^T$ and $H_2(q_j) = [0, 0, 0, 1]^T$ show the vehicle kinematic matrix, $M_\nu(q_j) \in \mathbb{R}^{2\times 2}$ is a symbol of the inertia matrix, $C_\nu(q_j, \nu_j) \in \mathbb{R}^{2\times 2}$ stands for a matrix of the Coriolis and centripetal forces, $D_\nu(q_j) \in \mathbb{R}^{2\times 2}$ denotes the damping matrix, $\tau_{\nu d} \in \mathbb{R}^2$ displays the external disturbances so that $\|\tau_{\nu d}\| \leq B_{\nu d}$ in which $B_{\nu d} \in \mathbb{R}^+$ shows an unknown constant, $B_\nu(q_j)$ corresponds to the inputs transformation matrix and, finally, $\tau_{sj} := [\tau_{sj1}, \tau_{sj2}]^T \in \mathbb{R}^2$ denotes a vector of saturated control force and torque inputs. The control input τ_s is defined by the following equation $\forall j = p, s$:

$$\tau_{sji} = \begin{cases} \text{sign}(\tau_{ji})\chi_{Mji} & , |\tau_{ji}| \geq \chi_{Mji}/m_{ji}, \forall i = 1, 2, \\ m_{ji}\tau_{ji} & , |\tau_{ji}| < \chi_{Mji}/m_{ji}, \end{cases} \tag{3}$$

in which τ_{sji}, τ_{ji}, and χ_{Mji} respectively show the saturated control input, unsaturated control input, and the actuators saturation limit. m_{ji} defines a ratio between τ_{sji} and τ_{ji}. Therefore, the saturation nonlinearity $d_{sji}(\tau_{ji}) = \tau_{sji} - \tau_{ji}$, that is a nonlinear-in-parameter (NLIP) function and cannot be implemented by the actuators, is defined as follows $\forall j = p, s$:

$$d_{sji} = \begin{cases} \text{sign}(\tau_{ji})\chi_{Mji} - \tau_{ji} & , |\tau_{ji}| \geq \chi_{Mji}/m_{ji}, \forall i = 1, 2, \\ (m_{ji} - 1)\tau_{ji} & , |\tau_{ji}| < \chi_{Mji}/m_{ji}. \end{cases} \tag{4}$$

C. Challenges and Control Objectives

In this paper, the main control objective is designing a coordinated tracking system for an Ackermann steering vehicle to track a reference vehicle which generates the desired trajectory such that the following challenging constraints and control objectives are satisfied:

R1: The preceding vehicle with the posture vector $q_p = [x_p, y_p, \varphi_p, \delta_p]^T$ and velocity vector $\nu_p = [v_p, \omega_p]^T$ tracks the succeeding or reference vehicle with the posture vector $q_s = [x_s, y_s, \varphi_s, \delta_s]^T$ and velocity vector $\nu_s = [v_s, \omega_s]^T$ so that the relative distance d and relative angle α in Fig. 1 between both vehicles exponentially tend to the zero neighbourhood with prescribed convergence speed, maximum overshoot/undershoot and steady-state tracking accuracy.

R2: It is of interest to design a proportional-integral-derivative control scheme to efficiently adjust the steady-state and transient performance characteristics.

R3: The controller only depends on the relative distance and angle measurements while velocity signals are not accessible for the feedback.

R4: The field-of-view of the relative angle sensor on the preceding vehicle is limited such that $|\beta| \leq \beta_m$ and consequently $|\alpha| \leq \alpha_m$ according to Fig. 1.

R5: The sensing range of the relative distance sensor on the preceding vehicle is restricted to $d_m \leq d \leq d_M$ where d_M and d_m are the maximum and minimum values of distance measurements, respectively.

R6: Both preceding and succeeding vehicles should keep their connectivity by maintaining their relative distance inside their communication ranges such that $d < R_c$ where R_c shows the maximum range of the data communication.

R7: The controller should prevent every possible collision between both vehicles according to predefined safe regions.

R8: The vehicle model is subjected to external disturbances, unmodeled dynamics and unknown parameters that should be compensated.

R9: The actuator saturation risk should be lessened as much as possible.

R10: The controller should be robust against the reference path curvature which is produced by the succeeding vehicle as much as possible.

R11: The controller should be robust against unknown vehicle's kinematic and dynamic parameters, external disturbances and unmodeled dynamics.

R12: The chattering on the control signals should be reduced as much as possible.

Designing a controller which solves all the above objectives $R1 - R12$ at the same time is very challenging. To this end, the following assumptions are crucial to be satisfied:

Assumption 1. The relative distance, angles and orientation of the preceding vehicle are measurable in real-time for the feedback and the vehicle is not equipped with velocity sensors.

Assumption 2. The posture and estimations of velocity and acceleration signals of the succeeding vehicle, i.e. q_s, $\hat{\nu}_s$ and $\dot{\hat{\nu}}_s$, are transmitted to the preceding vehicle via a transmitter with the communication range R_c.

Assumption 3. The external disturbance vector $\tau_{\nu d}$ is bounded in the sense that $\|\tau_{\nu d}\| \leq B_{\nu d}$ where $B_{\nu d} \in \mathbb{R}^+$ is an unknown constant.

D. Relative Distance and Orientation Errors

In this section, the relative position and orientation errors between both vehicles are changed from the earth-fixed frame $\{O_E, X_E, Y_E\}$ to the preceding vehicle's body-fixed frame $\{O_{Bp}, X_{Bp}, Y_{Bp}\}$ as follows:

$$\begin{bmatrix} e_x \\ e_y \\ e_\varphi \\ e_\delta \end{bmatrix} = \begin{bmatrix} cos\varphi_p & sin\varphi_p & 0 & 0 \\ -sin\varphi_p & cos\varphi_p & 0 & 0 \\ 0 & 0 & 1 & 0 \\ 0 & 0 & 0 & 1 \end{bmatrix} \begin{bmatrix} x_t - x_p \\ y_t - y_p \\ \varphi_s - \varphi_p \\ \delta_s - \delta_p \end{bmatrix}, \tag{5}$$

where (x_t, y_t) shows the position of the succeeding vehicle's transmitter in the earth-fixed frame as follows:

$$p_t(t) = \begin{bmatrix} x_t(t) \\ y_t(t) \end{bmatrix} = \begin{bmatrix} x_s(t) + r_t cos(\varphi_s(t) + \varphi_t) \\ y_s(t) + r_t sin(\varphi_s(t) + \varphi_t) \end{bmatrix}, \tag{6}$$

where (r_t, φ_t) shows the polar coordinates of the transmitter position on the succeeding vehicle's body-fixed frame $\{O_{Bs}, X_{Bs}, Y_{Bs}\}$. Now, the time derivative of (5) along (1)

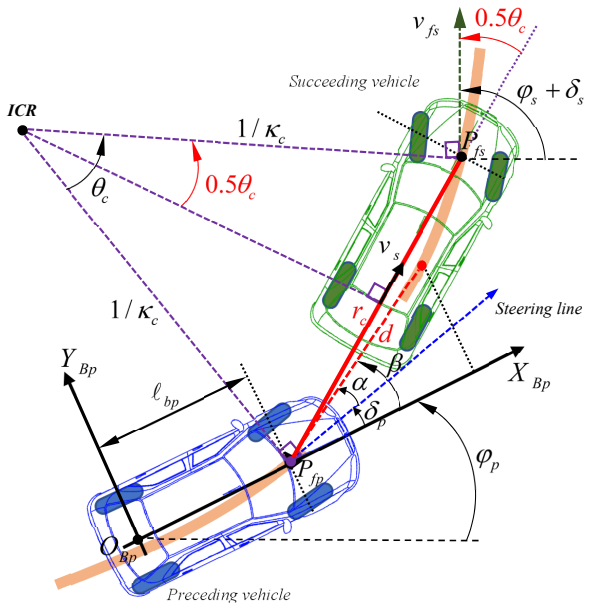

Fig. 2: The planar illustration of the path curvature.

and (6) results in

$$\begin{bmatrix} \dot{e}_x \\ \dot{e}_y \\ \dot{e}_\varphi \\ \dot{e}_\delta \end{bmatrix} = \begin{bmatrix} (e_y/\ell_{bp})tan\delta_p - 1 & 0 \\ -(e_x/\ell_{bp})tan\delta_p & 0 \\ -(1/\ell_{bp})tan\delta_p & 0 \\ 0 & -1 \end{bmatrix} \begin{bmatrix} v_p \\ \omega_p \end{bmatrix} + \begin{bmatrix} v_s cose_\varphi - r_t\dot{\varphi}_s sin(e_\varphi + \varphi_t) \\ v_s sine_\varphi + r_t\dot{\varphi}_s cos(e_\varphi + \varphi_t) \\ (v_s/\ell_{bs})tan\delta_s \\ \omega_s \end{bmatrix}. \quad (7)$$

Now, the relative distance d and the relative steering angle $\alpha = \beta - \delta_p$ in Fig. 1 are defined as follows to force the preceding vehicle to follow the succeeding vehicle.

$$r_e(t) = \begin{bmatrix} d_e(t) \\ \alpha_e(t) \end{bmatrix} = \begin{bmatrix} d - d_0 \\ \alpha - (\alpha_0 + 0.5\theta_c) \end{bmatrix} = \begin{bmatrix} \sqrt{(e_x - \ell_{bp})^2 + e_y^2} - d_0 \\ atan2(e_y, e_x - \ell_{bp}) - \delta_p - (\alpha_0 + 0.5\theta_c) \end{bmatrix}, \quad (8)$$

where $atan2(y, x)$ stands for the arc tangent function of y/x that generates the angle in $(-\pi, \pi]$. The parameter d_0 shows the desirable relative distance and α_0 represents the desirable relative orientation angle which is corrected by an intentional angle correction term $0.5\theta_c$ as shown by Fig. 2 to diminish unwanted deflection due to the path curvature of the succeeding vehicle [28] which is given by

$$\theta_c = 2arcsin\big(0.5 r_c \kappa_c(t)\big), \quad (9)$$

where $r_c = \|P_{fp} - P_{fs}\|$ is the distance between the point P_{fp} and the point P_{fs} in Fig. 2 whose coordinates are given by

$$P_{fk} = \begin{bmatrix} x_k(t) + \ell_{bk} cos(\varphi_k) \\ y_k(t) + \ell_{bk} sin(\varphi_k) \end{bmatrix}, \forall k = p, s. \quad (10)$$

The term $\kappa_c(t)$ in (9) defines the path curvature of the succeeding vehicle which is given by

$$\kappa_c = \frac{\dot{\varphi}_s + \dot{\delta}_s}{v_{fs}} = \frac{\dot{\varphi}_s + \omega_s}{\sqrt{v_s^2 + \ell_{bs}^2 \dot{\varphi}_s^2}} = \frac{\dot{\varphi}_s + \omega_s}{v_s/cos\delta_s} = \frac{1}{\ell_{bs}} sin\delta_s + \frac{\omega_s}{v_s} cos\delta_s \quad (11)$$

such that $v_{fs} \neq 0$ shows the linear velocity of the point P_{fs} on the succeeding vehicle. Because the steering angle is physically restricted such that $|\delta_s| \leq \delta_{s,max}$, $\forall \delta_{s,max} \in \mathbb{R}^+$, the path curvature is also limited such that $|\kappa_c| \leq \kappa_{c,max}$, $\forall \kappa_{c,max} \in \mathbb{R}^+$. As a result, the correction angle θ_c is bounded such that $|\theta_c| \leq \theta_{c,max}$, $\forall \theta_{c,max} \in \mathbb{R}^+$. To obtain the transformed kinematics, the time derivatives of (8) and (9) along (7) are given by

$$\dot{r}_e = J(d, \beta, \delta_p)\nu_p + \varpi(d, \beta, v_s, e_\varphi, \dot{\varphi}_s, \dot{\theta}_c), \quad (12)$$

where J and ϖ are derived as follows:

$$J = \begin{bmatrix} -cos\beta - sin\beta tan\delta_p & 0 \\ (sin\beta - cos\beta tan\delta_p)/d - tan\delta_p/\ell_{bp} & -1 \end{bmatrix}, \quad (13)$$

$$\varpi = \begin{bmatrix} v_s cos(e_\varphi - \beta) - r_t\dot{\varphi}_s sin(e_\varphi + \varphi_t - \beta) \\ v_s sin(e_\varphi - \beta)/d - 0.5\dot{\theta}_c - r_t\dot{\varphi}_s/d cos(e_\varphi + \varphi_t - \beta) \end{bmatrix}, \quad (14)$$

in which $\dot{\theta}_c$ denotes the change rate of the succeeding vehicle's path curvature that is given by

$$\dot{\theta}_c = \frac{r_c \dot{\kappa}_c}{\sqrt{1 - r_c^2 \kappa_c^2/4}}. \quad (15)$$

E. Relative Errors Constraints

To achieve the expected results $R1 - R7$ in Section II.C, the following error constraints should be considered in the control design process.

1) Limited Field-of-View and Singularity Avoidance: In order to ensure the system controllability and to prevent the singularity of the controller according to (13), the conditions $d \neq 0$ and $det(J) = cos\beta + sin\beta tan\delta_p \neq 0$ are necessary to be satisfied. This condition equivalently implies that $tan\beta\ tan\delta_p \neq -1$ which leads to $\beta - \delta_p \neq \pm\pi/2$ and subsequently $|\beta - \delta_p| < \pi/2$. On the other side, since $|\delta_p| < \delta_{p,max}$ and $|\beta| < \beta_m$ from $R4$, the following condition should be satisfied:

$$|\beta - \delta_p| < min\{\pi/2, \beta_m + \delta_{p,max}\} := \alpha_m. \quad (16)$$

Therefore, the following constraint is necessary to be considered:

$$-\alpha_m - \alpha_0 - 0.5\theta_c < \alpha_e < \alpha_m - \alpha_0 - 0.5\theta_c. \quad (17)$$

2) Limited Sensing Range, Collision Avoidance and Continuous Connectivity: Since (i) the sensing range of the onboard distance sensor on the preceding vehicle is restricted to $d_m \leq d \leq d_M$ according to $R5$; (ii) the collision between two vehicles should be avoided by ensuring $d > R_p + R_s$ in which R_p and R_s are the radii of safe areas around the vehicles in Fig. 1; and (iii) the communication between both vehicles should be maintained by considering $d < R_c$, the following overall condition is necessary to be satisfied for the relative range error:

$$\max\{R_p + R_s, d_m\} - d_0 < d_e < \min\{R_c, d_M\} - d_0. \quad (18)$$

To ensure the above conditions on the relative distance and angle between both vehicles, a constrained control technique is of interest.

F. Error Transformation

In this paper, the prescribed performance control strategy [26] is adopted to realize all the presented control objectives for the relative distance and orientation angle errors between both vehicles.

Definition 1 **[26]**. A bounded and smooth function $\rho_j(t)$: $\mathbb{R}^+ \to \mathbb{R}^+$ is called a performance one, if $\rho_j(t)$ is decreasing,

and $\lim_{t\to\infty}\rho_j(t)=\rho_{j\infty},\forall j=d,\alpha$.
One possible choice for $\rho_j(t)$ is given by

$$\rho_j(t)=\begin{cases}(\rho_{j0}-\rho_{j\infty})e^{-c_j h(t)}+\rho_{j\infty}, & \text{if} \quad t<T\\ \rho_{j\infty}, & \text{if} \quad t\geq T,\end{cases} \tag{19}$$

where $h(t)$ is an increasing time-function in such a way that $\lim_{t\to T}h(t)\to\infty\ \forall T\in\mathbb{R}^+$, $\rho_{j0}:=\rho_j(0)\geq\rho_j(t),\rho_{j\infty}$, and c_j denote positive constant scalars. To ensure (16)-(18), the tracking errors should be restricted by the following bounds:

$$\begin{aligned}&\rho_{ld}(t)=-a_d\rho_d(t)\leq d_e(t)\leq\rho_{ud}(t)=b_d\rho_d(t),\\&\rho_{l\alpha}(t)=-a_\alpha\rho_\alpha(t)\leq\alpha_e(t)\leq\rho_{u\alpha}(t)=b_\alpha\rho_\alpha(t),\end{aligned} \tag{20}$$

where $a_j,b_j\in\mathbb{R}^+$ are design scalars. To ensure (20), the following bounds on a_j and b_j should be satisfied:

$$\begin{cases}a_d<\big(d_0-\max\{R_p+R_s,d_m\}\big)/\rho_d(0),\\ b_d<\big(\min\{R_c,d_M\}-d_0\big)/\rho_d(0),\\ a_\alpha<\big(\alpha_m+\alpha_0+0.5\theta_c\big)/\rho_\alpha(0),\\ b_\alpha<\big(\alpha_m-\alpha_0-0.5\theta_c\big)/\rho_\alpha(0).\end{cases}$$

According to [26], a strictly increasing and smooth bijective nonlinear mapping is utilized bellow to ensure (20) on d_e and α_e:

$$\begin{aligned}&z_{ed}=T_d(\bar{d}_e(t)):\Omega_d\to\mathbb{R},T_d(0)=0,\\&z_{e\alpha}=T_\alpha(\bar{\alpha}_e(t)):\Omega_\alpha\to\mathbb{R},T_\alpha(0)=0,\end{aligned} \tag{21}$$

where $\bar{d}_e(t)=d_e(t)/\rho_d(t)$ and $\bar{\alpha}_e(t)=\alpha_e(t)/\rho_\alpha(t)$ denote modulated tracking error and $\Omega_d:=\{\bar{d}_e(t):\bar{d}_e\in(-a_d,b_d)\}$ and $\Omega_\alpha:=\{\bar{\alpha}_e(t):\hat{\alpha}_e\in(-a_\alpha,b_\alpha)\}$. Provided that $-a_d\rho_d(0)<d_e(0)<b_d\rho_d(0)$ and $-a_\alpha\rho_\alpha(0)<\alpha_e(0)<b_\alpha\rho_\alpha(0)$ and the controller ensures that $z_{ej}\in\mathcal{L}_\infty\ \forall t\geq 0$, then, $\bar{d}_e(t)\in\Omega_d$, $\bar{\alpha}_e(t)\in\Omega_\alpha$ and $\rho_{lj}(t)<j_e(t)<\rho_{uj}(t)$, $\forall j=d,\alpha$. On the basis of the properties mentioned above, the following nonlinear transformation from j_e to z_{ej} is introduced here [29]:

$$z_{ej}=T_j(\bar{j}_e)=tan\Big(\frac{\pi}{2}\times\frac{2\bar{j}_e-b_j+a_j}{b_j+a_j}\Big),\forall j=d,\alpha. \tag{22}$$

Then, the derivative of (22) with respect to the time gives

$$\dot{z}_{ej}=\frac{\partial T_j(\bar{j}_e)}{\partial\bar{j}_e}=\frac{\partial T_j(\bar{j}_e)}{\partial j_e}\frac{dj_e}{dt}+\Xi_j,\forall j=d,\alpha, \tag{23}$$

$$\Xi_j=\frac{\partial T_j(\bar{j}_e)}{\partial\rho_{uj}}\dot{\rho}_{uj}+\frac{\partial T_j(\bar{j}_e)}{\partial\rho_{lj}}\dot{\rho}_{lj}. \tag{24}$$

Now, one may achieve the following transformed error equation at the kinematic level by substituting (12) into (23):

$$\dot{z}_e=R(u)\nu_p+h(d,\beta,v_s,e_\varphi,\dot{\varphi}_s,\theta_c,\dot{\theta}_c,\rho_d,\dot{\rho}_d,\rho_\alpha,\dot{\rho}_\alpha), \tag{25}$$

where $z_e:=[z_{ed},z_{e\alpha}]^T$, $u:=[r_e^T,\rho^T,\delta_p]^T$ $\rho:=[\rho_d,\rho_\alpha]^T$, r_e is defined in (8) and R and h are derived as follows:

$$R(u)=\begin{bmatrix}\frac{\partial T_d}{\partial\hat{d}_e}\frac{J_{11}}{\rho_d} & \frac{\partial T_d}{\partial\hat{d}_e}\frac{J_{12}}{\rho_d}\\ \frac{\partial T_\alpha}{\partial\hat{\alpha}_e}\frac{J_{21}}{\rho_\alpha} & \frac{\partial T_\alpha}{\partial\hat{\alpha}_e}\frac{J_{22}}{\rho_\alpha}\end{bmatrix}, \tag{26}$$

$$h=\begin{bmatrix}\frac{1}{\rho_d}\frac{\partial T_d}{\partial\hat{d}_e}(\varpi_1-\frac{\dot{\rho}_d}{\rho_d}d_e)\\ \frac{1}{\rho_\alpha}\frac{\partial T_\alpha}{\partial\hat{\alpha}_e}(\varpi_2-\frac{\dot{\rho}_\alpha}{\rho_\alpha}\alpha_e)\end{bmatrix}, \tag{27}$$

where $J_{ij},\forall i,j=1,2$ and $\varpi_i,\forall i=1,2$ show elements of J and ϖ in (13) and (14) and $\partial T_j/\partial\bar{j}_e,\forall j=d,\alpha$ is given as follows:

$$\frac{\partial T_j(\bar{j}_e)}{\partial\bar{j}_e}=\frac{\pi}{a_j+b_j}sec^2\Big(\frac{\pi}{2}\times\frac{2\bar{j}_e-b_j+a_j}{a_j+b_j}\Big), \tag{28}$$

where it is clear that $\partial T_j/\partial\bar{j}_e>0$. As a result, provided that $z_{ej}\in\mathcal{L}_\infty$, then, constraints in (20) are fulfilled. Moreover, if z_{ej} converges to the origin vicinity as $t\to\infty$, j_e, $\forall j=d,\alpha$ tends to a small bound around the zero.

Assumption 4. The initial relative errors for the autonomous car are selected in such a way that

$$\rho_{lj}(0)<j_e(0)<\rho_{uj}(0),\forall j=d,\alpha. \tag{29}$$

G. Transformed Open-Loop Error Equation

Recall structural properties of (2) and write the velocity and acceleration of the preceding vehicle from (25) as follows:

$$\nu_p=R^{-1}\dot{z}_e-R^{-1}h, \tag{30}$$

$$\dot{\nu}_p=R^{-1}\ddot{z}_e-R^{-1}\dot{R}R^{-1}\dot{z}_e+R^{-1}\dot{R}R^{-1}h-R^{-1}\dot{h}. \tag{31}$$

Now, replace ν_p and $\dot{\nu}_p$ into (2), and multiply every side of the obtained equation by R^{-T} to get the following key dynamic model. In order to make the controller independent from the kinematic parameters in the matrix $B_\nu(q_p)$ in (2), we also add and subtract $R^{-T}\tau_p$ to the right-hand side of the resulting equation.

$$M(q)\ddot{z}_e+C(\varrho,\dot{z}_e)\dot{z}_e+D(q)\dot{z}_e-\xi(x_w)+\tau_d=R^{-T}\tau_p \tag{32}$$

where M, C, D, ξ, τ_d and B are given by

$$\begin{aligned}&M(q)=R^{-T}M_\nu(q_p)R^{-1},D(q)=R^{-T}D_\nu(q_p)R^{-1},\\&C=R^{-T}C_\nu(q_p,R^{-1}\dot{z}_e)R^{-1}-R^{-T}M_\nu(q_p)R^{-1}\dot{R}R^{-1},\\&\tau_d=R^{-T}\tau_{\nu d}(t),\\&\xi(x_w)=\xi_1(y)+\xi_2(x,\dot{z}_e),\\&\xi_1(y)=-R^{-T}C_\nu(q_p,R^{-1}h)R^{-1}h+D(q)h\\&\qquad+R^{-T}B_\nu(q_p)d_{sp}(\tau_p)+R^{-T}(B_\nu(q_p)-I_{2\times2})\tau_p,\\&\xi_2(x,\dot{z}_e)=R^{-T}C_\nu(q_p,R^{-1}\dot{z}_e)R^{-1}h+M(q)\dot{h}\\&-R^{-T}M_\nu R^{-1}\dot{R}R^{-1}h+R^{-T}C_\nu(q_p,R^{-1}h)R^{-1}\dot{z}_e,\end{aligned} \tag{33}$$

where $q:=[q_p^T,u^T]^T$, $\varrho:=[q^T,\dot{u}^T]^T$, $x_w=[x^T,\dot{z}_e^T]^T$, $x=[y^T,\ddot{\rho}^T,\ddot{v}_s,\dddot{\varphi}_s,\ddot{\theta}_c]^T$ and $y=[\tau_p^T,r_e^T,\theta_c,\dot{\theta}_c,\rho^T,\dot{\rho}^T,\varphi_p,\delta_p,v_s,\dot{v}_s,\dot{\varphi}_s,\ddot{\varphi}_s]^T$. Since $R(u)$ is full-rank, following properties are valid for (32):

Property 1. Inertia matrix satisfies $M(q)=M^T(q)>0$ and $\lambda_m\|y\|^2\leq y^TMy\leq\lambda_M\|y\|^2\ \forall y\in\mathbb{R}^2$ where $0<\lambda_m<\lambda_M<\infty$, and $\lambda_m:=min\{\lambda_{min}(M(q))\}$, $\lambda_M:=max\{\lambda_{max}(M(q))\}$.

Property 2. The conditions $D(q)=D^T(q)>0$ and $\lambda_d\|y\|^2\leq y^TDy\leq\lambda_D\|y\|^2\ \forall y\in\mathbb{R}^2$ hold true for damping matrix where $0<\lambda_d<\lambda_D<\infty$, and $\lambda_d:=min\{\lambda_{min}(D(q))\}$, $\lambda_D:=max\{\lambda_{max}(D(q))\}$.

Property 3. The matrix $C(\varrho, \dot{z}_e)$ satisfies the followings $\forall y, y_1, y_2 \in \mathbb{R}^2$:

1) $y^T(\dot{M}(q) - 2C(\varrho, \dot{z}_e))y = 0$;
2) $C(\varrho, y_1)y_2 = C(\varrho, y_2)y_1$;
3) $C(\varrho, y_1 + y_2)y = C(\varrho, y_1)y + C(\varrho, y_2)y$;
4) $\|C(\varrho, y_1)y_2\| \leq \lambda_c \|y_1\|\|y_2\|$ where $\lambda_c \in \mathbb{R}^+$.

III. MAIN RESULTS

A. Nonlinear PID-OFBC Design

In this section, a trajectory tracking control law is proposed to force the autonomous vehicle to track a desired trajectory with an arbitrary curvature. The following Lemmas and definition are necessary for the controller development and stability analysis.

Definition 2 [30]. A class of continuously differentiable functions $\mathcal{N}_f := [n_{f1}, ..., n_{fn}]^T$ whose elements are non-decreasing and locally Lipschitz and satisfying the following properties, are called saturation functions:

D1: *Boundedness*: $|n_{fi}(x)| \leq b_{fi} < \infty \ \forall x \in \mathbb{R}$;
D2: *Sector condition*: $xn_{fi}(x) > 0$ for $x \neq 0$ and $n_{fi}(0) = 0$;
D3: *Strictly increasing bounded derivative*: $0 < \frac{dn_{fi}(x)}{dx} < b_{pi} < \infty$ with $\frac{dn_{fi}(\infty)}{dx} = 0$.

Lemma 1 [31]. For a given function $n_{fi}(x)$ in Definition 2, the following properties hold true:

L1: $n_{fi}^2(x)/(2b_{pi}) \leq \int_0^x n_{fi}(z)dz \leq b_{pi}x^2/2 \ \forall x \in \mathbb{R}$;
L2: $\int_0^x n_{fi}(z)dz > 0, \ \forall x \neq 0$;
L3: $\int_0^x n_{fi}(z)dz \to \infty$, as $|x| \to \infty$.

Lemma 2 [31], [32]. There exist a class of saturation functions $\mathcal{S}_f := [s_{f1}, ..., s_{fn}]^T$ such that $|s_{fi}| \leq M_{fi}$ and satisfy the following relation $\forall \zeta \in \mathbb{R}^n, \gamma_t(t) > 0$ and $\forall c_s \in \mathbb{R}^+$:

$$\|\zeta\| - \zeta^T \mathcal{S}_f(\zeta/\gamma_t(t)) \leq c_s n \gamma_t(t). \tag{34}$$

Remark 1. The only difference between these two classes of saturation functions is that $\mathcal{S}_f(x)$ satisfies (34) while $\mathcal{N}_f(x)$ do not necessarily satisfy this inequality. Simple examples of $s_{fi}(x)$ and $n_{fi}(x)$ are respectively $s_{fi}(x) = tanh(x)$ with $c_s = 0.2785$ and $n_{fi}(x) = b_{pi}x/\sqrt{1 + b^2x^2}$ with $b := b_{pi}b_{fi}^{-1}$.

To commence the design, the following nonlinear PID-like filtered error variables are proposed in this paper:

$$\mu(t) = \dot{z}_e(t) + G_p \mathcal{N}_f(\hat{z}_e(t)) + G_i \sigma_i(t), \tag{35}$$

$$\eta(t) = \dot{\tilde{z}}_e(t) + G_p \mathcal{N}_f\big(\tilde{z}_e(t)\big) + G_i \delta_i(t), \tag{36}$$

$$\dot{\sigma}_i = -\ell_d \sigma_i + k_f \Big(\dot{z}_e(t) + G_p \mathcal{N}_f(\hat{z}_e(t)) + G_i \sigma_i \Big), \tag{37}$$

$$\dot{\delta}_i = -\ell_d \delta_i + k_f \Big(\dot{\tilde{z}}_e(t) + G_p \mathcal{N}_f\big(\tilde{z}_e(t)\big) + G_i \delta_i \Big), \tag{38}$$

where $\mathcal{N}_f(\hat{z}_e) := [n_{f1}(\hat{z}_{e1}), n_{f2}(\hat{z}_{e2})]^T$, $\mathcal{N}_f(\tilde{z}_e) := [n_{f1}(\tilde{z}_{e1}), n_{f2}(\tilde{z}_{e2})]^T$, $n_{fi}(\bullet)$ is defined in Definition 2, $\tilde{z}_e(t) = z_e(t) - \hat{z}_e(t)$ is the observation error, $G_p := diag[g_{p1}, g_{p2}] \in \mathbb{R}^{2\times 2}$ is a positive-definite gain matrix, $\sigma_i(t)$ and $\delta_i(t)$ represent integral actions in the above definitions of the error variables $\mu(t)$ and $\eta(t)$, and ℓ_d and k_f are some positive design parameters. By replacing (35) in (32), we get:

$$\begin{aligned} M(q)\dot{\mu} = &- C(\varrho, \dot{z}_e)\mu + R^{-T}\tau_p + \chi_c - D(q)\mu \\ &+ \xi(\hat{x}_w) - \tau_d, \end{aligned} \tag{39}$$

where χ_c is described by

$$\begin{aligned} \chi_c = &M(q)G_p \frac{\partial \mathcal{N}_f(\hat{z}_e)}{\partial \hat{z}_e}\big(\dot{z}_e - \dot{\tilde{z}}_e\big) - M(q)G_i\ell_d\sigma_i \\ &+ k_f M(q)G_i\mu + C(\varrho, \dot{z}_e)G_p\mathcal{N}_f\big(z_e(t) - \tilde{z}_e(t)\big) \\ &+ C(\varrho, \dot{z}_e)G_i\sigma_i + D(q)G_p\mathcal{N}_f\big(z_e(t) - \tilde{z}_e(t)\big) \\ &+ D(q)G_i\sigma_i + \xi(x_w) - \xi(\hat{x}_w). \end{aligned} \tag{40}$$

where

$$\frac{\partial \mathcal{N}_f(x)}{\partial \hat{z}_e} = diag\left[\frac{dn_{f1}(\hat{z}_{e1})}{d\hat{z}_{e1}}, \frac{dn_{f2}(\hat{z}_{e2})}{d\hat{z}_{e2}}\right], \tag{41}$$

and one may obtain the following bound for χ_c:

$$\|\chi_c\| \leq c_1\|Z\| + c_2\|Z\|^2, \tag{42}$$

in which $c_1, c_2 \in \mathbb{R}^+$ are unknown constants and Z is explained by

$$Z = [\mathcal{N}_f^T\big(z_e - \tilde{z}_e\big), \sigma_i^T, \mu^T, \mathcal{N}_f^T\big(\tilde{z}_e\big), \delta_i^T, \eta^T]^T. \tag{43}$$

Then, the following novel nonlinear PID-like controller is proposed in this paper:

$$\begin{aligned} \tau_p = &R^T\Big(- K_p\dot{\hat{z}}_e(t) - K_pG_p\mathcal{N}_f(\hat{z}_e) + K_pG_p\mathcal{N}_f(\tilde{z}_e) \\ &- K_pG_i\kappa_i(t) - \hat{\Theta}(t)\Phi(\hat{x}_w) - \hat{p}(t)\mathcal{S}_f\big((\hat{\mu} + \hat{\eta})/\gamma_t\big)\Big), \end{aligned} \tag{44}$$

where $K_p := diag[k_{p1}, k_{p2}] \in \mathbb{R}^{2\times 2}$ is a positive-definite gain matrix, $\mathcal{S}_f(\bullet)$ depicts the saturation function that is described in Lemma 2, $\hat{\Theta}(t)\Phi(\hat{x}_w)$ shows the NN control action which is defined later and $\hat{\mu} + \hat{\eta}$ displays an estimation of $\mu + \eta$ which is given by

$$\hat{\mu} + \hat{\eta} = \dot{\hat{z}}_e + G_p\mathcal{N}_f(\hat{z}_e) + G_p\mathcal{N}_f(\tilde{z}_e) + G_i(\hat{\sigma}_i + \hat{\delta}_i). \tag{45}$$

in which $\hat{\sigma}_i + \hat{\delta}_i$ represents an estimation of $\sigma_i + \delta_i$ and it is updated by

$$\dot{\hat{\sigma}}_i + \dot{\hat{\delta}}_i = -\ell_d(\hat{\sigma}_i + \hat{\delta}_i) + k_f(\hat{\mu} + \hat{\eta}). \tag{46}$$

The term $\kappa_i = \sigma_i - \delta_i$ in (44) is accessible due to the absence of $\dot{z}_e$ in its computation and it reconstructs the nonlinear integral action which is updated by the following designed law:

$$\dot{\kappa}_i = -\ell_d\kappa_i + k_f\Big(\dot{\hat{z}}_e + G_p\mathcal{N}_f(\hat{z}_e) - G_p\mathcal{N}_f(\tilde{z}_e) + G_i\kappa_i\Big). \tag{47}$$

The following learning laws are presented to obtain $\hat{p}(t)$ and $\hat{\Theta}(t)$ as follows in (44):

$$\dot{\hat{\Theta}} = \text{Proj}_{\hat{\Theta}}\left(\Gamma_\Theta(\hat{\mu} + \hat{\eta})\Phi^T(\hat{x}_w) - \Gamma_\Theta\sigma_\Theta\hat{\Theta}\right), \tag{48}$$

$$\dot{\hat{p}} = \text{Proj}_{\hat{p}}\Big(\gamma_p(\hat{\mu}+\hat{\eta})^T\mathcal{S}_f\big((\hat{\mu}+\hat{\eta})/\gamma_t(t)\big) - \gamma_p\sigma_p\hat{p}\Big), \quad (49)$$

$$\dot{\gamma}_t(t) = -c_\gamma\gamma_t(t) + g_0(t) + g_1\|\mathcal{N}_f(\hat{z}_e)\|, \quad \gamma_t(0) > 0, \quad (50)$$

where $g_1 \in \mathbb{R}^+$ and $g_0(t) > 0$ is a time function that satisfies

$$\lim_{t\to\infty}\int_0^t g_0(s)ds = g_{0\infty} < \infty \quad (51)$$

where $g_{0\infty} \in \mathbb{R}^+$, $\hat{x}_w = [\hat{x}^T, \dot{\hat{z}}_e^T]^T$, in which $\hat{x} = [\hat{y}^T, \ddot{\rho}^T, \dddot{\hat{v}}_s, \ddot{\hat{\varphi}}_s]^T$ and $\hat{y} = [\tau_p^T, r_e^T, \rho^T, \dot{\rho}^T, \varphi_p, \delta_p, \hat{v}_s, \dot{\hat{v}}_s, \hat{\varphi}_s, \dot{\hat{\varphi}}_s]^T$ where $\hat{\bullet}_s$ denotes the measured or estimated signals which are received from the succeeding vehicle, $\Phi(\hat{x}_w)$ is a vector for radial basis functions, $\hat{\Theta}(0) \in \Omega_\Theta := \{\hat{\Theta} \in \mathbb{R}^{n_o\times n_h} : tr\{\hat{\Theta}^T\hat{\Theta}\} \le \Theta_m\}$ and $\hat{p}(0) \in \Omega_p := \{\hat{p} \in \mathbb{R} : 0 \le \hat{p} \le p_m\}$ and $\Gamma_\Theta \in \mathbb{R}^{n_o\times n_o}$ and $\gamma_p, \sigma_\Theta, \sigma_p, c_\gamma \in \mathbb{R}^+$ are adaptive laws parameters. Because the chattering often occurs in the transient phase [33], the update rule (50) leads to a bigger boundary layer thickness since $\|\mathcal{N}_f(\hat{z}_e)\|$ is large in the transient response and, as a result, we have a smaller chattering. On the other hand, at the steady-state response, a smaller boundary layer thickness is obtained since $\|\mathcal{N}_f(\hat{z}_e)\|$ is close to the origin and, as a result, we may have a better tracking accuracy at the steady-state. We employ $g_0(t) > 0$ to maintain the thickness of the boundary layer even when $\hat{z}_e \to 0$.

Then, we propose the following nonlinear velocity estimator in this paper:

$$\hat{\nu}_p = R^{-1}\dot{\hat{z}}_e - R^{-1}h, \quad (52)$$

$$\dot{\hat{z}}_e = \xi_o + G_p\mathcal{N}_f(\tilde{z}_e) + \ell_d\tilde{z}_e - G_i\kappa_i, \quad (53)$$

$$\dot{\xi}_o = \ell_d G_p\mathcal{N}_f(\tilde{z}_e) - G_p\frac{\partial\mathcal{N}_f(\hat{z}_e)}{\partial\hat{z}_e}\dot{\hat{z}}_e, \quad (54)$$

where $\ell_d \in \mathbb{R}^+$ shows the velocity observer gain and $\xi_o(0) = -G_p\mathcal{N}_f(\tilde{z}_e(0)) - \ell_d\tilde{z}_e(0) + G_i\kappa_i(0)$ and $\tilde{z}_e(0) = 0$ show its initial values. It should be noted that the above observer-controller scheme is based on a Lyapunov-based systematic design which will be presented in the sequel.

Remark 2: The employment of the saturation function $\mathcal{N}_f(\bullet)$ in the above observer definition effectively reduces the unwanted peaking in the estimated velocity signals. As a result, a smoother transient response will be obtained.

Remark 3. Main novel features of the proposed control system are listed as follows: (i) the filtered error variables (35)-(38) helped us to construct a PID-like controller to reach the objectives R1-R2 in Section II.C; (ii) velocity and acceleration measurements are not required by the proposed observer (52)-(54) and the objective R3 is satisfied; (iii) the PPC is effectively applied to the relative errors dynamics between both vehicles to get the objectives R1 and R4-R7; (iv) an operational combination of ARC scheme and NNs in the last two terms of (44) effectively addresses the objectives R8 and R11; (v) the objective R9 is satisfied by limiting the amplitudes of the estimation and tracking errors and by estimating and compensating the actuator saturation nonlinearity $d_{sji}(\tau_{ji})$, $\forall i = 1, 2, j = p, s$ in (4) by using NN; (vi) the inclusion of the path curvature θ_c in the definition of α_e in (8) and its compensation by RBFNN helps us to reach R10; and finally (vii) the chattering risk is diminished by using (50) and R12 is obtained.

Remark 4. It is worth noting that the sole aim of designing observer in this paper is to estimate the speed of the preceding vehicle $\hat{\nu}_p$. As can be inferred from (52)-(53), this requires calculation of the velocity signal $\dot{\hat{z}}_e$ in (52), which in turn needs the value of the observation error $\tilde{z}_e$ in (53) and (54). In this case, the observation error $\tilde{z}_e$ can be calculated easily as Assumption 1 allows us to measure the relative distance and angles and orientation of the preceding vehicle. The transformed version of these variables is represented by the state z_e and can be measured using (8), (22) and real sensors such as laser range finder. However, based on a realistic assumption, the relative velocity signal $\dot{z}_e$ is not measurable via sensors and the aim of observer design is to estimate this variable using the velocity observer (52)-(54). Thus, the estimated state $\hat{z}_e$ is generated by integrating the observer itself and as such the observation error $\tilde{z}_e = z_e - \hat{z}_e$ is known to calculate or estimate the relative velocity $\dot{\hat{z}}_e$. It is possible to optionally use each of these variables, i.e. $\hat{z}_e$, $\dot{\hat{z}}_e$ and z_e, in the controller design as needed. Although the only purpose of our proposed observer in (53)-(54) is the estimation of the velocity signal $\dot{\hat{z}}_e$, it is also generating the estimated state $\hat{z}_e$.

Fig. 3 shows a detailed controller block diagram.

B. Stability and Error Convergence Analysis

In this section, the stability of the proposed controller-observer system is examined on the basis of Lyapunov's direct method. To derive the closed-loop control error equations, the approximation error for the expression $\hat{\mu}+\hat{\eta}$ in (44) is computed as follows:

$$\tilde{\mu}+\tilde{\eta} := \mu+\eta-(\hat{\mu}+\hat{\eta}) = 2\Big(I - k_f G_i(sI+\ell_d I)^{-1}\Big)^{-1}\dot{\tilde{z}}_e, \quad (55)$$

where $\ell_d > k_f\lambda_{max}\{G_i\}$. The above approximation error is bounded as follows:

$$\|\tilde{\mu}+\tilde{\eta}\| \le c_3\|Z\|, \quad (56)$$

where $c_3 \in \mathbb{R}^+$ is an unknown constant. Now, consider the derivative of (53) with respect to the time along (54) as follows:

$$\begin{aligned}\ddot{\tilde{z}}_e =& \ell_d G_p\mathcal{N}_f(\tilde{z}_e) - G_p\frac{\partial\mathcal{N}_f(\hat{z}_e)}{\partial\hat{z}_e}\dot{\hat{z}}_e \\ &+ G_p\frac{\partial\mathcal{N}_f(\tilde{z}_e)}{\partial\tilde{z}_e}\dot{\tilde{z}}_e + \ell_d\dot{\tilde{z}}_e - G_i\dot{\kappa}_i, \end{aligned} \quad (57)$$

which is equivalent to

$$\dot{\mu}(t) = \dot{\eta}(t) + \ell_d\eta(t) - \ell_d G_i\delta_i(t). \quad (58)$$

By replacing (44) in (39), one achieves the following closed-loop error equation:

$$\begin{aligned}M(q)\dot{\mu} =& -C(\varrho,\dot{z}_e)\mu - K_p\dot{\hat{z}}_e - K_pG_p\mathcal{N}_f(\hat{z}_e) + K_pG_p\mathcal{N}_f(\tilde{z}_e) \\ &- K_pG_i\kappa_i - \hat{\Theta}(t)\Phi(\hat{x}_w) - \hat{p}\mathcal{S}_f\big((\hat{\mu}+\hat{\eta})/\gamma_t\big) \\ &+ \chi_c - D(q)\mu + \xi(\hat{x}_w) - \tau_d. \end{aligned} \quad (59)$$

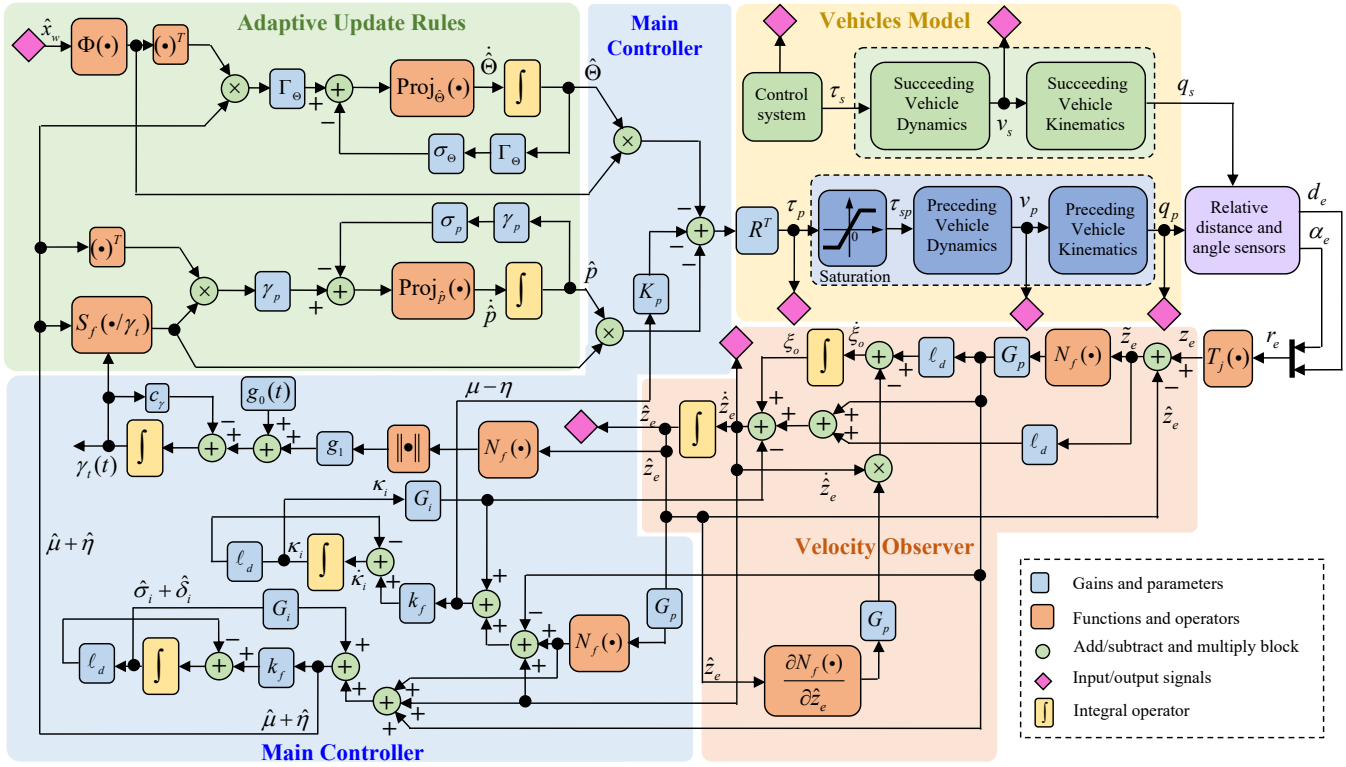

Fig. 3: A detailed block diagram of the proposed control system.

Then, the estimation property of the radial basis function NN is adopted to write that

$$\xi(\hat{x}_w) = \Theta^* \Phi(\hat{x}_w) + \epsilon_w(\hat{x}_w), \forall \hat{x}_w \in \Omega_Z \subset \mathbb{R}^{n_i}, \quad (60)$$

where $n_i := dim\{x_w\}$, and the ideal network weights matrix is explained by

$$\Theta^* := \underset{\hat{\Theta} \subset \mathbb{R}^{n_h}}{arg\ min} \left\{ \underset{\hat{x}_w \in \Omega_{x_w}}{sup} \|\xi(\hat{x}_w) - \hat{\Theta}\Phi(\hat{x}_w)\| \right\},$$

in which $\Phi(\hat{x}_w) = [\phi_1(\hat{x}_w), ..., \phi_{n_h}(\hat{x}_w)]^T$, $\|\Theta^*\|_F \leq \Theta_M$ where $\phi_i(\hat{x}_w) = exp(-\|\hat{x}_w - \mu_{wi}\|^2/\lambda_{wi}^2)$ describes ith Gaussian basis function, n_h shows the hidden-layer nodes number and λ_{wi} and μ_{wi} denote the standard deviation and center vector, respectively, whose descriptions are found in [34] in detail. Now, by taking (60) into account and considering that

$$\dot{\hat{z}}_e + G_p \mathcal{N}_f(\hat{z}_e) - G_p \mathcal{N}_f(\tilde{z}_e) + G_i(\sigma_i - \delta_i) := \mu - \eta, \quad (61)$$

from (35) and (36), the closed-loop error equation are obtained as follows:

$$\begin{aligned} M(q)\dot{\mu} = &- C(\varrho, \dot{z}_e)\mu - K_p(\mu - \eta) + \tilde{\Theta}\Phi(\hat{x}_w) \\ &- \hat{p}\mathcal{S}_f\big((\hat{\mu} + \hat{\eta})/\gamma_t\big) + \chi_c - D(q)\mu \\ &+ \epsilon_w(\hat{x}_w) - \tau_d, \end{aligned} \quad (62)$$

where $\tilde{\Theta} := \Theta^* - \hat{\Theta}$ denotes the NN weights matrix approximation error. By recalling (58) and (62), the observer error dynamic equation is achieved as

$$\begin{aligned} M(q)\dot{\eta} = &- C(\varrho, \dot{z}_e)\eta - M(q)\ell_d\eta - K_p(\mu - \eta) \\ &+ M(q)\ell_d G_i \delta_i + \tilde{\Theta}\Phi(\hat{x}_w) + \chi_o \\ &- \hat{p}\mathcal{S}_f\big((\hat{\mu} + \hat{\eta})/\gamma_t\big) + \epsilon_w(\hat{x}_w) - \tau_d, \end{aligned} \quad (63)$$

where χ_o includes additional terms which is explained by

$$\chi_o := -D(q)\mu - C(\varrho, \dot{z}_e)\mu + C(\varrho, \dot{z}_e)\eta + \chi_c, \quad (64)$$

where χ_o is bounded by the following statement:

$$\|\chi_o\| \leq c_4\|Z\| + c_5\|Z\|^2, \quad (65)$$

in which $c_4, c_5 \in \mathbb{R}^+$ are unknown parameters and Z was defined in (43).

Now, main results are wrapped up by the following theorem in this paper:

Theorem 1. Take into account the autonomous vehicle's models described by (1) and (2) in which Assumptions $1-4$ hold true. Then, the proposed control laws (44)-(54) under the following gain conditions for $0 < \epsilon < 1$

$$\begin{aligned} \lambda_{min}\{K_p G_p^2\} >& 0.5\lambda_{max}\{K_p G_p^2\} \\ &+ \Lambda_{k_p g_p} + \lambda_{max}\{K_p G_p G_i\}, \end{aligned} \quad (66)$$

$$\begin{aligned} \lambda_{min}\{K_p + D(q)\} >& 0.5\epsilon\Lambda_{k_p g_p} + 0.5k_f\epsilon \\ &+ 0.5(c_1 + c_2)/\epsilon, \end{aligned} \quad (67)$$

$$\ell_d > max\{L_{dm1}, L_{dm2}, L_{dm3}\}, \quad (68)$$

$$c_\gamma > 0.5\epsilon + 0.5g_1\epsilon \quad (69)$$

where $L_{dmi}, i = 1, 2, 3$ are defined as follows:

$$L_{dm1} = 0.5k_f/\epsilon + 0.5\epsilon\lambda_{max}\{K_p G_p G_i\}, \quad (70)$$

$$L_{dm2} = \frac{0.5k_f/\epsilon + \epsilon\lambda_{max}\{K_p G_p G_i\}}{1 - 0.5\epsilon\lambda_{max}\{M(q)G_i\}}, \quad (71)$$

$$L_{dm3} = \frac{\lambda_{k_p} + 0.5k_f\epsilon + \epsilon\Lambda_{k_pg_p} + 0.5(c_4+c_5)/\epsilon}{\lambda_m - 0.5\lambda_{max}\{M(q)G_i\}/\epsilon}, \quad (72)$$

and $\lambda_{k_p} := \lambda_{min}\{K_p\}$, $\Lambda_{k_pg_p} := \lambda_{max}\{K_pG_p\}$, $\lambda_m := min\{\lambda_{min}(M(q))\}$, ensures that (i) the relative tracking errors, i.e. r_e, the position and velocity estimation errors, i.e. $\tilde{z}_e$ and $\dot{\tilde{z}}_e$, are semi-globally uniformly ultimately bounded (SGUUB) and tend to the zero neighbourhood exponentially with prescribed performance criteria; (ii) all available signals in the designed closed-loop control system stay bounded, and (iii) the following attraction region

$$R_A = \left\{ \vartheta \in \mathbb{R}^m \middle| \|\vartheta\| < \sqrt{\frac{2a_m - (c_1+c_3+c_4)\epsilon}{(c_2+c_5)\epsilon(\lambda_\vartheta/\lambda_Z)}} \right\}, \quad (73)$$

(with $m = 13 + n_o n_h$) may be expanded freely to contain every possible initial condition by a fair tuning of the control parameters where $a_m, \lambda_Z, \lambda_\vartheta, c_j, \forall j = 1,\dots,5$ and ϑ will be clarified later in the proof section.

Proof: Consider the Lyapunov function below:

$$\begin{aligned}\mathcal{L} =& k_{p1}g_{p1}\int_0^{\hat{z}_{e1}} n_{f1}(z)dz + k_{p2}g_{p2}\int_0^{\hat{z}_{e2}} n_{f2}(z)dz \\ &+ k_{p1}g_{p1}\int_0^{\tilde{z}_{e1}} n_{f1}(z)dz + k_{p2}g_{p2}\int_0^{\tilde{z}_{e2}} n_{f2}(z)dz \\ &+ 0.5\big(\mu^T M(q)\mu + \eta^T M(q)\eta + \delta_i^T\delta_i + \sigma_i^T\sigma_i\big) \\ &+ 0.5\text{tr}\left\{\tilde{\Theta}^T\Gamma_\Theta^{-1}\tilde{\Theta}\right\} + 0.5\gamma_p^{-1}\tilde{p}^2 + 0.5\gamma_t^2(t), \end{aligned} \quad (74)$$

with $\tilde{p} = p^* - \hat{p}$ and applying Lemma 1, it can be proved that

$$\lambda_Z\|Z\|^2 \le \lambda_\upsilon\|\upsilon\|^2 \le \mathcal{L}(t) \le \lambda_\vartheta\|\vartheta\|^2, \quad (75)$$

where Z was defined in (43), $\upsilon = [Z^T, \tilde{\theta}_{11}, ..., \tilde{\theta}_{n_on_h}, \tilde{p}, \gamma_t]^T$, $\vartheta = [\hat{z}_e^T, \sigma_i^T, \mu^T, \tilde{z}_e^T, \delta_i^T, \eta^T, \tilde{\theta}_{11}, ..., \tilde{\theta}_{n_on_h}, \tilde{p}, \gamma_t]^T$, and

$$\begin{aligned}&\lambda_Z = 0.5min\{1, k_{p1}g_{p1}/b_{p1}, k_{p2}g_{p2}/b_{p2}, \lambda_m\}, \\ &\lambda_\upsilon = 0.5min\{2\lambda_Z, \lambda_{min}\{\Gamma_\Theta^{-1}\}, \gamma_p^{-1}\}, \\ &\lambda_\vartheta = 0.5max\{1, k_{p1}g_{p1}b_{p1}, k_{p2}g_{p2}b_{p2}, \lambda_M, \lambda_{max}\{\Gamma_\Theta^{-1}\}, \gamma_p^{-1}\}. \end{aligned} \quad (76)$$

By taking the time derivative of (74) along (62) and (63) and employing item 1 of Property 3 and (35)-(36), one gets

$$\begin{aligned}\dot{\mathcal{L}} =& -\mathcal{N}_f^T(\hat{z}_e)K_pG_p^2\mathcal{N}_f(\hat{z}_e) - \mathcal{N}_f^T(\tilde{z}_e)K_pG_p^2\mathcal{N}_f(\tilde{z}_e) - \ell_d\sigma_i^T\sigma_i \\ &- \ell_d\delta_i^T\delta_i - \mu^T(K_p + D(q))\mu - \eta^T(\ell_dM(q) - K_p)\eta \\ &+ \mathcal{N}_f^T(\hat{z}_e)K_pG_p\mu - \mathcal{N}_f^T(\hat{z}_e)K_pG_p\eta + \mathcal{N}_f^T(\hat{z}_e)K_pG_p^2\mathcal{N}_f(\tilde{z}_e) \\ &- \mathcal{N}_f^T(\hat{z}_e)K_pG_pG_i\sigma + \mathcal{N}_f^T(\hat{z}_e)K_pG_pG_i\delta + k_f\sigma_i^T\mu \\ &+ (\mu+\eta)^T\tilde{\Theta}\Phi(\hat{x}_w) - \hat{p}(\mu+\eta)^T\mathcal{S}_f\big((\hat{\mu}+\hat{\eta})/\gamma_t\big) \\ &+ (\mu+\eta)^T(\epsilon_w(\hat{x}_w) - \tau_d) + \mathcal{N}_f^T(\tilde{z}_e)K_pG_p\eta \\ &- \mathcal{N}_f^T(\tilde{z}_e)K_pG_pG_i\delta_i + k_f\delta_i^T\eta + \ell_d\eta^TM(q)G_i\delta_i \\ &- \text{tr}\left\{\tilde{\Theta}^T\Gamma_\Theta^{-1}\dot{\hat{\Theta}}\right\} - \gamma_p^{-1}\tilde{p}\dot{\hat{p}} + \mu^T\chi_c + \eta^T\chi_o \\ &- c_\gamma\gamma_t^2 + g_0(t)\gamma_t + g_1\|\mathcal{N}_f(\hat{z}_e)\|\gamma_t. \end{aligned}$$

By considering that $ab \le 0.5a^2/\epsilon + 0.5\epsilon b^2\ \forall\epsilon \in \mathbb{R}^+$ and recalling (42) and (65), it can be verified that

$$\begin{aligned}\|\mu^T\chi_c + \eta^T\chi_o\| \le& 0.5(c_1+c_2)\|\mu\|^2/\epsilon + 0.5(c_1+c_4)\epsilon\|Z\|^2 \\ &+ 0.5(c_4+c_5)\|\eta\|^2/\epsilon + 0.5(c_2+c_5)\epsilon\|Z\|^4. \end{aligned} \quad (77)$$

By substituting (55) and applying (77), the following inequality after some mathematical manipulation can be achieved:

$$\begin{aligned}\dot{\mathcal{L}} \le& -a_1\|\mathcal{N}_f(\hat{z}_e)\|^2 - a_2\|\sigma_i\|^2 - a_3\|\mu\|^2 - a_4\|\mathcal{N}_f(\tilde{z}_e)\|^2 \\ &- a_5\|\delta_i\|^2 - a_6\|\eta\|^2 + 0.5(c_1+c_4)\epsilon\|Z\|^2 \\ &+ 0.5(c_2+c_5)\epsilon\|Z\|^4 + (\hat{\mu}+\hat{\eta})^T\tilde{\Theta}\Phi(\hat{x}_w) \\ &+ (\tilde{\mu}+\tilde{\eta})^T\Omega - \hat{p}(\hat{\mu}+\hat{\eta})^T\mathcal{S}_f\big((\hat{\mu}+\hat{\eta})/\gamma_t\big) \\ &+ (\hat{\mu}+\hat{\eta})^T(\epsilon_w - \tau_d) - \text{tr}\left\{\tilde{\Theta}^T\Gamma_\Theta^{-1}\dot{\hat{\Theta}}\right\} - \gamma_p^{-1}\tilde{p}\dot{\hat{p}} \\ &- \big(c_\gamma - 0.5\epsilon - 0.5g_1\epsilon\big)\gamma_t^2 + 0.5g_0^2(t)/\epsilon, \end{aligned} \quad (78)$$

in which $a_i, \forall i = 1,\dots,6$ are given by

$$\begin{cases} a_1 := \lambda_{min}\{K_pG_p^2\} - \lambda_{max}\{K_pG_p\}/\epsilon - 0.5g_1/\epsilon \\ \qquad - 0.5\lambda_{max}\{K_pG_p^2\}/\epsilon - \lambda_{max}\{K_pG_pG_i\}/\epsilon, \\ a_2 := \ell_d - 0.5k_f/\epsilon - 0.5\epsilon\lambda_{max}\{K_pG_pG_i\}, \\ a_3 := \lambda_{min}\{K_p + D(q)\} - 0.5\epsilon\lambda_{max}\{K_pG_p\} - 0.5k_f\epsilon \\ \qquad - 0.5(c_1+c_2)/\epsilon, \\ a_4 := \lambda_{min}\{K_pG_p^2\} - 0.5\epsilon\lambda_{max}\{K_pG_p^2\} \\ \qquad - 0.5\lambda_{max}\{K_pG_pG_i\}/\epsilon - 0.5\lambda_{max}\{K_pG_p\}/\epsilon, \\ a_5 := \ell_d - 0.5k_f/\epsilon - \epsilon\lambda_{max}\{K_pG_pG_i\} \\ \qquad - 0.5\epsilon\lambda_{max}\{\ell_dM(q)G_i\}, \\ a_6 := \lambda_{min}\{\ell_dM(q) - K_p\} - 0.5k_f\epsilon - \epsilon\lambda_{max}\{K_pG_p\} \\ \qquad - 0.5(c_4+c_5)/\epsilon - 0.5\lambda_{max}\{\ell_dM(q)G_i\}/\epsilon, \end{cases}$$

and Ω in (78) is expressed as

$$\Omega = \tilde{\Theta}\Phi(\hat{x}_w) - \hat{p}\mathcal{S}_f\big((\hat{\mu}+\hat{\eta})/\gamma_t\big) + \epsilon_w - \tau_d. \quad (79)$$

By considering (56), $\|\Theta^*\|_F \le \Theta_M$, $\|\epsilon_w - \tau_d\| \le p^*$, and the projection operator property, it is easy to prove that

$$\begin{aligned}\|\Omega\| \le& \sqrt{\Theta_m n_h} + \Theta_M\sqrt{n_h} \\ &+ \sqrt{2}max\{M_{f1}, M_{f2}\}p_m + p^* := \Omega_M. \end{aligned} \quad (80)$$

Recalling $\hat{p} = p^* - \tilde{p}$ and replacing (48), (49), and (80) in (78), and applying $ab \le 0.5a^2/\epsilon + 0.5\epsilon b^2\ \forall\epsilon \in \mathbb{R}^+$ one gets:

$$\begin{aligned}\dot{\mathcal{L}} \le& -a_z\|Z\|^2 + 0.5c_3\Omega_M^2/\epsilon + \|\hat{\mu}+\hat{\eta}\|p^* \\ &+ (\tilde{p}-p^*)(\hat{\mu}+\hat{\eta})^T\mathcal{S}_f\big((\hat{\mu}+\hat{\eta})/\gamma_t\big) + (\hat{\mu}+\hat{\eta})^T\tilde{\Theta}\Phi(\hat{x}_w) \\ &- \text{tr}\left\{\tilde{\Theta}^T\Gamma_\Theta^{-1}\text{Proj}_{\hat{\Theta}}\left(\Gamma_\Theta(\hat{\mu}+\hat{\eta})\Phi^T(\hat{x}_w) - \Gamma_\Theta\sigma_\Theta\hat{\Theta}\right)\right\} \\ &- \gamma_p^{-1}\tilde{p}\text{Proj}_{\hat{p}}\Big(\gamma_p(\hat{\mu}+\hat{\eta})^T\mathcal{S}_f\big((\hat{\mu}+\hat{\eta})/\gamma_t\big) - \gamma_p\sigma_p\hat{p}\Big), \end{aligned} \quad (81)$$

where a_z is defined by

$$a_z = a_m - 0.5(c_1+c_3+c_4)\epsilon - 0.5(c_2+c_5)\epsilon\|Z\|^2, \quad (82)$$

in which $a_m = \min\{a_j\}_{j=1}^6$. Now, by considering Lemma 2 and the following inequalities:

$$(\hat{\mu}+\hat{\eta})^T\tilde{\Theta}\Phi - \text{tr}\left\{\tilde{\Theta}^T\text{Proj}_{\hat{\Theta}}\left((\hat{\mu}+\hat{\eta})\Phi^T\right)\right\} \leq 0, \quad (83)$$

$$\tilde{p}(\hat{\mu}+\hat{\eta})^T\mathcal{S}_f\big((\hat{\mu}+\hat{\eta})/\gamma_t\big) - \gamma_p^{-1}\tilde{p}\text{Proj}_{\hat{p}}\Big(\gamma_p(\hat{\mu}+\hat{\eta})^T\mathcal{S}_f\big((\hat{\mu}+\hat{\eta})/\gamma_t\big)\Big) \leq 0, \quad (84)$$

$$\|\hat{\mu}+\hat{\eta}\|p^* - p^*(\hat{\mu}+\hat{\eta})^T\mathcal{S}_f\big((\hat{\mu}+\hat{\eta})/\gamma_t\big) \leq 2c_s p^*\gamma_t, \quad (85)$$

$$\sigma_p\tilde{p}\hat{p} \leq -(1-0.5/\epsilon_p^2)\sigma_p\tilde{p}^2 + 0.5\epsilon_p^2\sigma_p p^{*2}, \forall\epsilon_p \in \mathbb{R}, \quad (86)$$

$$\sigma_\Theta\text{tr}\{\tilde{\Theta}^T\hat{\Theta}\} \leq -(1-0.5/\epsilon_\Theta^2)\sigma_\Theta\|\tilde{\Theta}\|_F^2 + 0.5\epsilon_\Theta^2\sigma_\Theta\|\Theta^*\|_F^2, \quad \forall\epsilon_\Theta \in \mathbb{R}, \quad (87)$$

the inequality (81) is expressed as follows:

$$\dot{\mathcal{L}}(t) \leq -a\|\upsilon(t)\|^2 + \gamma(t), \quad (88)$$

where a and $\gamma(t)$ are given by

$$a := \min\{a_z, (1-0.5/\epsilon_p^2)\sigma_p, (1-0.5/\epsilon_\Theta^2)\sigma_\Theta\},$$

$$\gamma(t) := 0.5\epsilon_p^2\sigma_p p^{*2} + 0.5\epsilon_\Theta^2\sigma_\Theta\|\Theta^*\|_F^2 + 2c_s p^*\gamma_t(t) + 0.5c_3\Omega_M^2/\epsilon + 0.5g_0^2(t)/\epsilon. \quad (89)$$

As a result, if the gains K_p, G_p, and ℓ_d are selected sufficiently large such that the inequalities (66)-(68) are satisfied and scalars $a_j, \forall j = 1,\ldots,6$ and a_z remain positive, then, the following condition could be derived for the closed-loop system stability:

$$a_m > 0.5(c_1+c_3+c_4)\epsilon + 0.5(c_2+c_5)\epsilon\|Z\|^2. \quad (90)$$

By considering the analysis above, $\dot{\mathcal{L}}(t)$ in (88) is strictly negative-definite when $\|\upsilon\|$ is outside the compact set $\Omega_\upsilon := \{\upsilon(t) : 0 \leq \|\upsilon\| \leq \sqrt{\gamma_\infty/a}\}$ in which $\gamma_\infty := \lim_{t\to\infty}\gamma(t)$. This indicates that the elements of $\upsilon(t)$ are decreasing outside the compact set Ω_υ and one infers from (75) that $\lambda_Z\|Z\|^2 \leq \mathcal{L}(t) \leq \mathcal{L}(0) \leq \lambda_\vartheta\|\vartheta(0)\|^2$, $\forall t \geq 0$, leading to $\|Z\|^2 \leq (\lambda_\vartheta/\lambda_Z)\|\vartheta(0)\|^2, \forall t \geq 0$. Subsequently, a sufficient condition for (90) is given by $a_m > 0.5(c_1+c_3+c_4)\epsilon + 0.5(c_2+c_5)\epsilon(\lambda_\vartheta/\lambda_Z)\|\vartheta(0)\|^2$. This shows that attraction region R_A in (73) could be chosen arbitrarily large to contain every desired initial condition via a suitable choice of the control parameters K_p, G_p, and ℓ_d. Thereafter, the closed-loop control system is SGUUB such that $\mathcal{N}_f(\hat{z}_e)$, $\mathcal{N}_f(\tilde{z}_e)$, μ, η, σ_i, δ_i $\tilde{\theta}_{11}$,...,$\tilde{\theta}_{n_o n_h}$, $\tilde{p}, \gamma_t(t) \in \mathcal{L}_\infty$ and the tracking and observation errors tend to their own residual sets containing the zero. From (35)-(36), $\dot{z}_e$, $\dot{\tilde{z}}_e \in \mathcal{L}_\infty$. Thus, from (44), and Assumption 3, it is clear that $\hat{z}_e$, $\dot{\hat{z}}_e$, $\hat{p}$, $\hat{\theta}_{11}$,...,$\hat{\theta}_{n_o n_h}$, $\tau \in \mathcal{L}_\infty$. The discussion above shows that z_e and $\tilde{z}_e$ are SGUUB and converge to small residual sets including the origin. Since $z_{ej}(t) \in \mathcal{L}_\infty$ and $\rho_{lj}(0) < j_e(0) < \rho_{uj}(0)$, $\forall t \geq 0$, one concludes that $\rho_{lj}(t) < j_e(t) < \rho_{uj}(t)$, $\forall j = d, \alpha$ which indicates that $z_e(t)$ exponentially tends to small compact set containing zero with a prescribed performance. This finalizes the proof. □

IV. SIMULATION EXAMPLE

A. Simulation Results

In this section, computer simulations have been performed and their results are displayed to examine the effectiveness of the proposed control system for our cooperative control problem. The first autonomous vehicle which is called the succeeding vehicle is forced to move along a reference path and the second vehicle that is called preceding vehicle should follow the first vehicle while satisfying all the control objectives $R1 - R12$ in Section II.C. The matrices describing dynamic model of the system are given by $M_\nu(q_j) = H^T(q_j)M_q(q_j)H(q_j)$, $C_\nu(q_j,\nu_j) = H^T(q_j)M_q(q_j)\dot{H}(q_j) + H^T(q_j)C_q(q_j, H(q_j)\nu_j)H(q_j)$, $D_\nu(q_j) = H^T(q_j)D_q(q_j)H(q_j)$ and $B_\nu(q_j) = H^T(q_j)B_q(q_j)$, $\forall j = p, s$ for which

$$M_q = \begin{bmatrix} m_{cj} & 0 & -a_j sin\varphi_j & 0 \\ 0 & m_{cj} & a_j cos\varphi_j & 0 \\ -a_j sin\varphi_j & a_j cos\varphi_j & I_{cj}+I_{fj} & I_{fj} \\ 0 & 0 & I_{fj} & I_{fj} \end{bmatrix}, \quad (91)$$

$$C_q\dot{q}_j = \begin{bmatrix} -a_j\dot{\varphi}_j^2 cos\varphi_j \\ -a_j\dot{\varphi}_j^2 sin\varphi_j \\ 0 \\ 0 \end{bmatrix}, \quad B_q = \begin{bmatrix} cos\varphi_j & 0 \\ sin\varphi_j & 0 \\ \ell_b sin\delta_j cos\delta_j & 0 \\ 0 & 1 \end{bmatrix}, \quad (92)$$

where $a_j := m_{cj}\ell_{cj}$ and $D_q(q_j) = diag[5,5,2,2]$. The vehicle parameters are listed in Table I. The controller parameters are given in Table II. One possible choice for the parameters of (50) is $g_0(t) = 100e^{-0.01t}$, $g_1 = 5$ and $c_\gamma = 1$. The nonlinear functions in the control laws (44) are selected as follows:

$$n_{fi}(z_i) = z_i/\sqrt{1+z_i^2}, i = 1,2,$$
$$\mathcal{S}_f\big((\hat{\mu}+\hat{\eta})/\gamma_t\big) = (\hat{\mu}+\hat{\eta})/\sqrt{\gamma_t^2 + \|\hat{\mu}+\hat{\eta}\|^2}. \quad (93)$$

It is assumed that the control torque and force are saturated according to $|\tau_{pi}| \leq 50, \forall i = 1,2$. Also, the communication range of the succeeding vehicle is limited inside a circle with the radius $R_c = 10m$. A transmitter is placed on the succeeding vehicle at the polar coordinates $(r_t, \varphi_t) = (0.25, -\pi/6)$. The safety regions around the preceding and succeeding vehicles are defined as circles with radii $R_p = 0.6m$ and $R_s = 1.25m$, respectively. Moreover, the field-of-view and range of the onboard sensor on the preceding vehicle are limited such that $\alpha_m = 75°$, $d_m = 0.25m$ and $d_M = 6m$. Both vehicles start at the initial postures $q_p = [0, 1.5, 0, 0]^T$ and $q_s = [2.5, 5.5, 0, 0]^T$ at the same time. The succeeding vehicle is commanded to move along a trajectory generated by the following open-loop torque command:

$$\tau_s = [\tau_{s1}, \tau_{s2}]^T, \tau_{s1} = 8,$$
$$\tau_{s2} = 0.4sech^2(0.2(t-50)) - 0.9sech^2(0.2(t-110)) + 0.9sech^2(0.2(t-170)) - 0.9sech^2(0.2(t-190)). \quad (94)$$

The preceding vehicle should keep the desired distance $d_0 = 1.9m$ and the relative angle $\alpha_0 = 0$ with respect to the suc-

ceeding vehicle while it is subjected to the disturbance vector $\tau_{\nu d}(t) = \tau_{dp}(t) + f_p(\nu_p)$ where $\tau_{dp}(t) = 20sin(t/20)[1,1]^T$ and the vector $f_p(\nu_p) = F_c sign(\nu_p) + F_v \nu_p$ simulates Coulomb and viscous frictions. The constants $F_c = 0.5$ and $F_v = 0.75$ are considered. It is assumed that the dynamic parameters for the succeeding vehicle are unknown. The desired path curvature and speed variations are generated by the succeeding vehicle according to the reference command (94). A random noise is added to the vehicle states by using $randn(\bullet)$ function to reflect the sensor noise. Numerical results are illustrated in Figs. 4-10. To highlight the salient features of the proposed controller, the output-feedback linear PID controller in [25] has been simulated and compared with our proposed constrained output-feedback nonlinear PID controller. Figures 4 and 5 show the $x-y$ trajectories of the preceding and succeeding vehicles for both controllers. As shown by these figures, the preceding vehicle tracks and keeps the succeeding vehicle continuously inside its limited field-of-view while avoiding any collision. Figures 6 and 7 illustrate that the relative distance and angle errors converge to the origin vicinity inside the performance bounds. The time evolution of unconstrained errors, i.e z_e, is shown in Fig. 8. Figure 9 shows that the velocity estimation errors converge to the vicinity of the zero very fast while no unwanted peaking phenomena is observed. Figure 10 shows the time evolutions of the weights and parameter estimations which are bounded and smooth. Fig. 11 confirms that the proposed controller avoids every possible collision between both vehicles throughout the path. However, the controller [25] experiences a possible collision because the preceding vehicle enters the safe regions, i.e. $d < R_p + R_s$. Due to the lack of space, other signals have been omitted here. As confirmed by the figures mentioned above, the preceding vehicle is following the succeeding one very accurately while satisfying all the control objectives mentioned in Section II.C. However, the controller [25] is missing the defined requirements and objectives.

TABLE I: Model parameters description and their values in Fig. 1.

Parameter	Description	value
Driving wheels radius	r_j	0.2 m
Distance between two rear wheels	$2b_j$	1 m
The Length of the vehicle	ℓ_{vj}	1.7 m
Distance between front and rear wheels	ℓ_{bj}	1.2 m
Distance between O_{Bj} and P_{cj}	ℓ_{cj}	0.55 m
The vehicle mass	m_{cj}	30 kg
The moment of inertia about vertical axis through P_{cj}	I_{cj}	5 kgm^2
The moment of inertia of the vehicle	I_{fj}	10 kgm^2

B. A Comparative Study on Robustness and Performance

As stated in Section I, all the previous works including [8]-[25] suffer from at least one of the shortcomings (i)-(viii). The proposed controller have successfully addressed such drawbacks in theory in Sections II and III and they are also shown by simulations. To further show the superior performance and robustness of the proposed controller with respect to the controller in [25], the amount of disturbance signal is increased

TABLE II: PID controller, observer, NN and PPF parameters.

Control gain	Attributed values	Control gain	Attributed values
K_p	$20I_{2\times2}$	G_p	$2I_{2\times2}$
G_i	$0.5I_{2\times2}$	ℓ_d	10
k_f	0.25	n_h	9
Γ_Θ	0.1	γ_p	0.25
σ_Θ	$0.1\Gamma_\Theta$	σ_p	$0.25\gamma_p$
γ_t	100	μ_{wi}	[-4,-3,-2,-1,0,1,2,3,4]
λ_{wi}	10	Θ_m	20
p_m	10	c_d, c_α	0.5,0.5
$\rho_{d0}, \rho_{\alpha 0}$	$2, 1$	$\rho_{j\infty}$	0.08
a_d, b_d	$0.825, 2.05$	a_α, b_α	$1.309 \pm 0.5\theta_c$

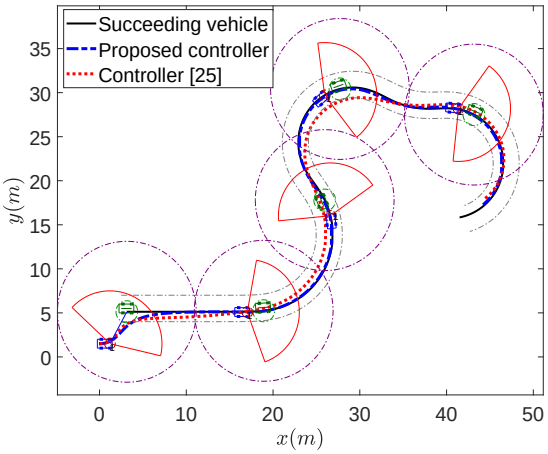

Fig. 4: The $x-y$ trajectories of both vehicles for the proposed controller and controller [25].

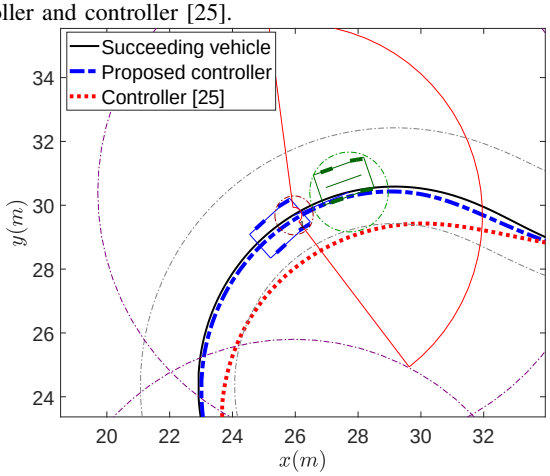

Fig. 5: A magnified view of $x-y$ trajectories for both vehicles.

up to three times with respect to the previous simulation and the result is shown by Fig. 12. This figure confirms the absolute competency of the proposed controller with respect to the previous output-feedback linear PID controller in [25]. The torque control signals are also plotted for both controllers in Fig. 13 which shows that the proposed method successfully prevents the control signals from the saturation. Another simulation has been carried out to compare the controller in [25] and proposed controller in a quantitative way and the results based on some performance criteria are given by Table III to demonstrate the effective performance of the proposed controller. This table compares both controllers based on the following criteria: (i) $rms(e_i)$, $\forall i = 1, 2$ stands for the errors root mean square for the measure of *average tracking performance*; (ii) $e_{M,i} := max_t\{|e_i(t)|\}$ gives the errors maximum

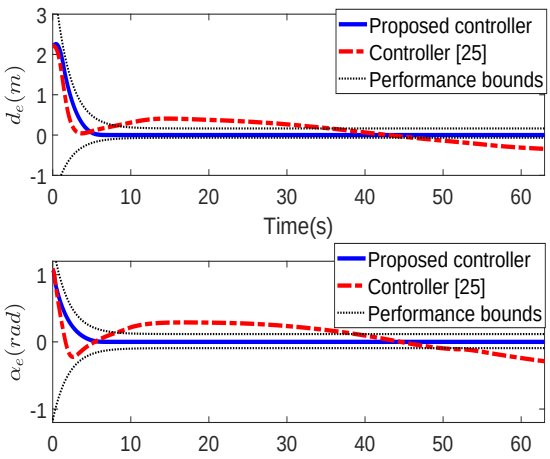

Fig. 6: Constrained relative distance and angle errors between preceding and succeeding vehicles for the proposed controller and controller [25].

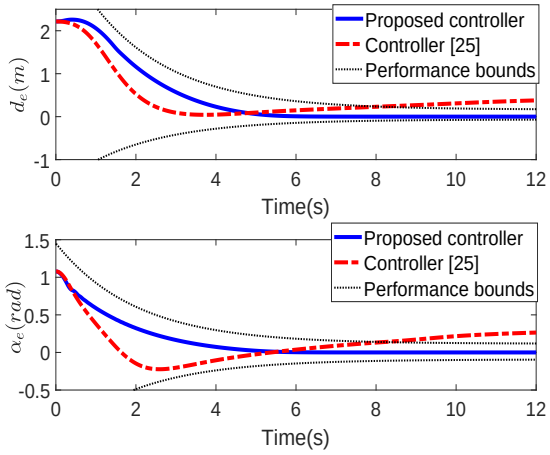

Fig. 7: An enlarged view of constrained relative distance and relative angle errors for the proposed controller and controller [25].

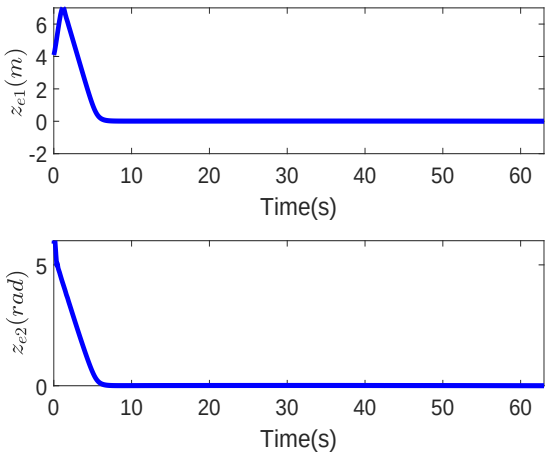

Fig. 8: The evolution of transformed errors with respect to the time.

absolute value for the evaluation of *transient performance* and (iii) $e_{f,i} := max_{T_f-T_L\leq t\leq T_f}\{|e_i(t)|\}$ represents the errors maximum absolute value within the last $T_L = 5$ seconds for the assessment of the *final tracking accuracy* and T_f shows the total program run-time. The table confirms that the proposed nonlinear PID-type controller performs quite better than the PID controller in [25].

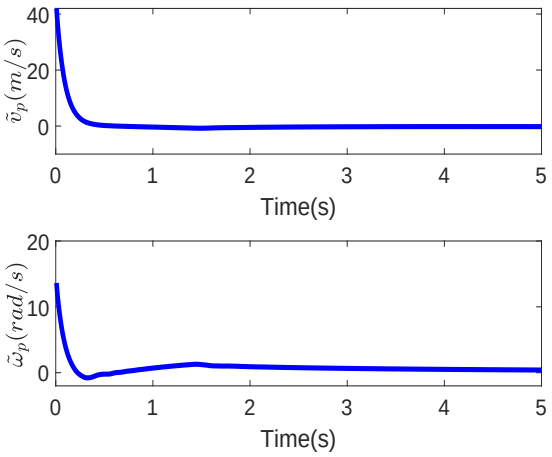

Fig. 9: Linear and angular velocity estimation errors for the proposed observer.

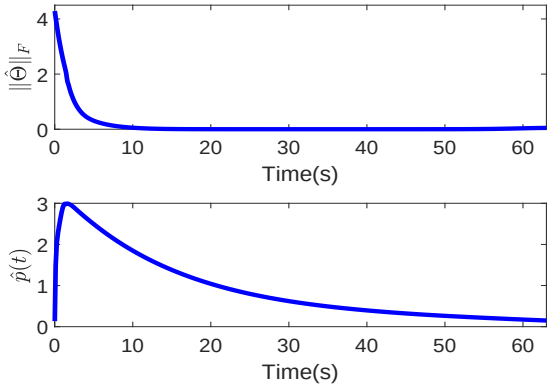

Fig. 10: The estimation of Frobenius norm of weights matrix Θ and unknown parameter p.

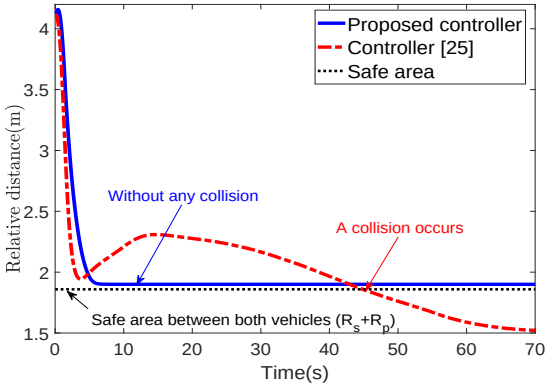

Fig. 11: The relative distance d and collision possibility between both vehicles.

V. Conclusion, Future Works and Limitations

The output-feedback control of two cooperative autonomous vehicles with limited sensing range and limited field-of-view sensors was addressed in this paper. To preserve continuous communication between vehicles while preventing every possible collision and compensating the path curvature, the relative distance and angle errors between both vehicles were transformed to construct an Euler-Lagrange error dynamic equation in terms of the transformed errors. Then, a NN adaptive robust saturated PID-like controller with a saturated nonlinear velocity observer was proposed to force the preceding vehicle to follow the succeeding vehicle with a

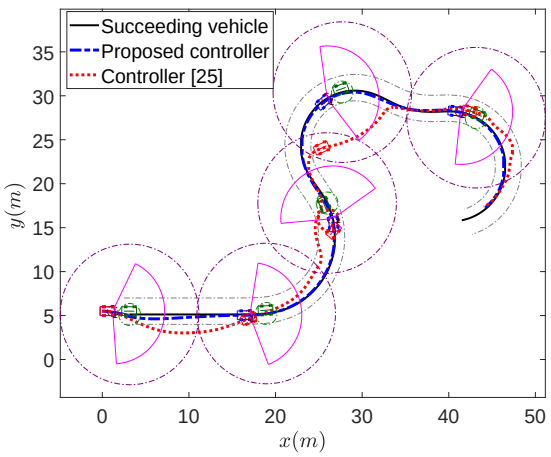

Fig. 12: The $x-y$ trajectories of both vehicles for the proposed controller and controller [25] for a very large disturbance.

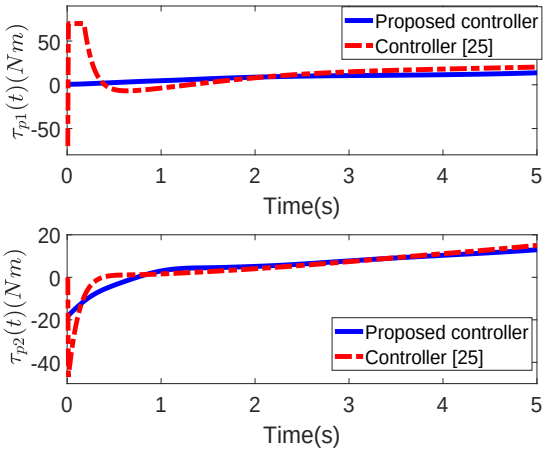

Fig. 13: The control signals for the proposed controller and controller [25] for a very large disturbance in the presence of actuator saturation.

limited torque and without velocity measurements. A semi-global UUB stability of the controller-observer system was successfully analyzed using the Lyapunov's direct method. Simulation results confirmed that the proposed controller is a successful candidate for the cooperative vehicle-following problem under some realistic conditions and assumptions. An extension of the present work to a group of N autonomous vehicles shows our future research program. An experimental evaluation of the proposed controller on a real autonomous vehicle is another direction of future studies. The main limitations of the presented method are listed as follows which are left to be addressed by interested readers in the future:

- Sensor errors and communication delays may result in a poor performance or even instability of the proposed controller in practice.
- Initial relative errors between the vehicles are restricted to a compact set which prevents the global stability.
- The velocity and acceleration signals of the succeeding vehicle need to be available for the preceding vehicle.
- The lateral slippage of the preceding vehicle may lead to a poor performance or even instability which is neglected in this paper.

TABLE III: The quantitative evaluation of both controllers' performances in both transient and steady-state responses.

Performance Index	Proposed controller	Controller [25]
rms(e_ℓ) (m)	1.48	3.8
rms(e_α) (rad.)	0.47	3.3
$e_{M,\ell}$ (m)	2.2	2.2
$e_{M,\alpha}$ (rad.)	1.08	1.08
$e_{f,\ell}$ (m)	7.8×10^{-5}	0.26
$e_{f,\alpha}$ (rad.)	5.1×10^{-5}	0.26

REFERENCES

[1] Z. Lian, P. Shi, C.-C. Lim, and X. Yuan, "Fuzzy-model-based lateral control for networked autonomous vehicle systems under hybrid cyber-attacks," *IEEE Transactions on Cybernetics*, vol. 53, no. 4, pp. 2600–2609, 2023.

[2] Y. Guan, Y. Ren, Q. Sun, S. E. Li, H. Ma, J. Duan, Y. Dai, and B. Cheng, "Integrated decision and control: Toward interpretable and computationally efficient driving intelligence," *IEEE Transactions on Cybernetics*, vol. 53, no. 2, pp. 859–873, 2023.

[3] Q. Sun, X. Wang, G. Yang, Y.-H. Chen, and F. Ma, "Adaptive robust formation control of connected and autonomous vehicle swarm system based on constraint following," *IEEE Transactions on Cybernetics*, vol. 53, no. 7, pp. 4189–4203, 2023.

[4] C. Chatzikomis, A. Sorniotti, P. Gruber, M. Zanchetta, D. Willans, and B. Balcombe, "Comparison of path tracking and torque-vectoring controllers for autonomous electric vehicles," *IEEE Transactions on Intelligent Vehicles*, vol. 3, no. 4, pp. 559–570, 2018.

[5] H. Taghavifar, "Neural network autoregressive with exogenous input assisted multi-constraint nonlinear predictive control of autonomous vehicles," *IEEE Transactions on Vehicular Technology*, vol. 68, no. 7, pp. 6293–6304, 2019.

[6] A.-T. Nguyen, C. Sentouh, H. Zhang, and J.-C. Popieul, "Fuzzy static output feedback control for path following of autonomous vehicles with transient performance improvements," *IEEE Transactions on Intelligent Transportation Systems*, vol. 21, no. 7, pp. 3069–3079, 2020.

[7] A. Bono, G. Fedele, and G. Franzè, "A swarm-based distributed model predictive control scheme for autonomous vehicle formations in uncertain environments," *IEEE Transactions on Cybernetics*, vol. 52, no. 9, pp. 8876–8886, 2022.

[8] Y. Hwang, C. M. Kang, and W. Kim, "Robust nonlinear control using barrier Lyapunov function under lateral offset error constraint for lateral control of autonomous vehicles," *IEEE Transactions on Intelligent Transportation Systems*, vol. 23, no. 2, pp. 1565–1571, 2022.

[9] Y. Ma, J. Chen, J. Wang, Y. Xu, and Y. Wang, "Path-tracking considering yaw stability with passivity-based control for autonomous vehicles," *IEEE Transactions on Intelligent Transportation Systems*, vol. 23, no. 7, pp. 8736–8746, 2022.

[10] Z. Qin, L. Chen, M. Hu, and X. Chen, "A lateral and longitudinal dynamics control framework of autonomous vehicles based on multi-parameter joint estimation," *IEEE Transactions on Vehicular Technology*, vol. 71, no. 6, pp. 5837–5852, 2022.

[11] X. Zhou, Z. Wang, H. Shen, and J. Wang, "Robust adaptive path-tracking control of autonomous ground vehicles with considerations of steering system backlash," *IEEE Transactions on Intelligent Vehicles*, vol. 7, no. 2, pp. 315–325, 2022.

[12] Z. Zhou, F. Zhu, D. Xu, B. Chen, S. Guo, and Y. Dai, "Event-triggered multi-lane fusion control for 2-D vehicle platoon systems with distance constraints," *IEEE Transactions on Intelligent Vehicles*, pp. 1–14, 2022.

[13] Y. Huang, S. Z. Yong, and Y. Chen, "Stability control of autonomous ground vehicles using control-dependent barrier functions," *IEEE Transactions on Intelligent Vehicles*, vol. 6, no. 4, pp. 699–710, 2021.

[14] Y. Zhang, W. Wang, W. Wang, C. Yang, and Y. Zhang, "An adaptive constrained path following control scheme for autonomous electric vehicles," *IEEE Transactions on Vehicular Technology*, vol. 71, no. 4, pp. 3569–3578, 2022.
[15] Y. Liang, Y. Li, A. Khajepour, Y. Huang, Y. Qin, and L. Zheng, "A novel combined decision and control scheme for autonomous vehicle in structured road based on adaptive model predictive control," *IEEE Transactions on Intelligent Transportation Systems*, vol. 23, no. 9, pp. 16 083–16 097, 2022.
[16] Z. Yang, J. Huang, H. Yin, D. Yang, and Z. Zhong, "Path tracking control for underactuated vehicles with matched-mismatched uncertainties: An uncertainty decomposition based constraint-following approach," *IEEE Transactions on Intelligent Transportation Systems*, vol. 23, no. 8, pp. 12 894–12 907, 2022.
[17] S. Cui, Y. Xue, M. Lv, B. Yao, and B. Yu, "Cooperative constrained control of autonomous vehicles with nonuniform input quantization," *IEEE Transactions on Vehicular Technology*, vol. 71, no. 11, pp. 11 431–11 442, 2022.
[18] Y. Xiao, X. Zhang, X. Xu, X. Liu, and J. Liu, "Deep neural networks with koopman operators for modeling and control of autonomous vehicles," *IEEE Transactions on Intelligent Vehicles*, vol. 8, no. 1, pp. 135–146, 2023.
[19] Q. Zhang and G. Guo, "Prescribed-time cooperative control of connected and autonomous vehicles on rough roads," *IEEE Transactions on Vehicular Technology*, pp. 1–12, 2024.
[20] Jing Zhang, Q. Gao, J. Tian, F. Cui, and T. Wang, "Car-following model based on spatial expectation effect in connected vehicle environment: modeling, stability analysis and identification," *Physica A: Statistical Mechanics and its Applications*, vol. 641, p. 129747, 2024.
[21] D. Chu, H. Li, C. Zhao, and T. Zhou, "Trajectory tracking of autonomous vehicle based on model predictive control with PID feedback," *IEEE Transactions on Intelligent Transportation Systems*, vol. 24, no. 2, pp. 2239–2250, 2023.
[22] Tianyi Chen, S. Gong, M. Wang, X. Wang, Y. Zhou, and B. Ran, "Stochastic capacity analysis for a distributed connected automated vehicle virtual car-following control strategy," *Transportation Research Part C: Emerging Technologies*, vol. 152, p. 104176, 2023.
[23] J. Wang, J. Guo, K. Li, and H. Zheng, "Distributed adaptive event-triggered control of connected automated vehicle platoon systems with spoofing cyber attacks," *IEEE Transactions on Vehicular Technology*, pp. 1–11, 2024.
[24] C. Dong, Y. Chen, H. Wang, D. Ni, X. Shi, and K. Lyu, "An evolutionary learning framework of lane-changing control for autonomous vehicles at freeway off-ramps," *IEEE Transactions on Vehicular Technology*, vol. 72, no. 2, pp. 1611–1628, 2023.
[25] K. Shojaei, "Neural adaptive PID formation control of car-like mobile robots without velocity measurements," *Advanced Robotics*, vol. 31, no. 18, pp. 947–964, 2017.
[26] C. P. Bechlioulis and G. A. Rovithakis, "Robust adaptive control of feedback linearizable mimo nonlinear systems with prescribed performance," *IEEE Transactions on Automatic Control*, vol. 53, no. 9, pp. 2090–2099, 2008.
[27] P. Ioannou and B. Fidan, *Adaptive control tutorial*. Philadelphia: SIAM, 2006.
[28] A. Bayuwindra, E. Lefeber, J. Ploeg, and H. Nijmeijer, "Extended look-ahead tracking controller with orientation-error observer for vehicle platooning," *IEEE Transactions on Intelligent Transportation Systems*, vol. 21, no. 11, pp. 4808–4821, 2020.
[29] M. Chen, "Disturbance attenuation tracking control for wheeled mobile robots with skidding and slipping," *IEEE Transactions on Industrial Electronics*, vol. 64, no. 4, pp. 3359–3368, 2017.
[30] M. Namvar, "A class of globally convergent velocity observers for robotic manipulators," *IEEE Transactions on Automatic Control*, vol. 54, no. 8, pp. 1956–1961, 2009.
[31] K. Shojaei, "Coordinated saturated output-feedback control of an autonomous tractor-trailer and a combine harvester in crop-harvesting operation," *IEEE Transactions on Vehicular Technology*, vol. 71, no. 2, pp. 1224–1236, 2022.
[32] ——, "Intelligent coordinated control of an autonomous tractor-trailer and a combine harvester," *European Journal of Control*, vol. 59, pp. 82–98, 2021.
[33] M.-S. Chen, Y.-R. Hwang, and M. Tomizuka, "A state-dependent boundary layer design for sliding mode control," *IEEE Transactions on Automatic Control*, vol. 47, no. 10, pp. 1677–1681, 2002.
[34] F. L. Lewis, D. M. Dawson, and C. T. Abdallah, *Robot manipulator control: theory and practice*. New York: Marcel Dekker, 2004.

Khoshnam Shojaei was born in Esfahan, Iran. He received the B.S., M.S. and Ph.D. degrees (with distinction) from the Iran University of Science and Technology (IUST), Tehran, Iran, in 2004, 2007, and 2011, respectively, all in electrical engineering. Currently, he is an Associate Professor with the Najafabad Branch, Islamic Azad University, Najafabad, Iran. His research interests include the adaptive control of nonlinear systems, control of autonomous robots including land, air and ocean vehicles, navigation of mobile robots, and multiagent systems.

Allahyar Montazeri (Member, IEEE) received the B.S. degree in Electrical Engineering from the University of Tehran, Iran, in 2000, and the M.Sc. and Ph.D. degrees in Electrical Engineering from the Iran University of Science and Technology, Tehran, in 2002 and 2009, respectively. From 2010 to 2011, he was a Research Fellow at the Fraunhofer Institute, Germany, and continued his research with Fraunhofer IDMT and the Control Engineering Group at Ilmenau University from 2011 to 2013. He has also held visiting research positions with the Control Engineering Group at ETH Zürich, Switzerland, and the Chemical Engineering Group at the Norwegian University of Science and Technology (NTNU), Trondheim, Norway. Since 2013, he has been with the School of Engineering at Lancaster University, UK, where he is currently an Associate Professor. He received the ERCIM Fellowship in 2010 and the Humboldt Research Award in 2011. He is a Fellow of the Higher Education Academy. His research has been supported by various UK research councils and industrial partners, including the Engineering and Physical Sciences Research Council (EPSRC) and National Nuclear Laboratory. He currently serves as Editor-in-Chief of the Journal of Intelligent and Fuzzy Systems, and as Associate Editor for Frontiers in Robotics and AI and Science Progress. He is a member of the Executive Board of the UK Automatic Control Network and serves on the IFAC Technical Committees on "Adaptive and Learning Systems" and "Modelling, Identification, and Signal Processing." His research interests include control theory and digital signal processing, with a focus on adaptive signal processing and control, robust control, system identification (linear and nonlinear), estimation theory, and evolutionary computing and optimization. His work has applications in active noise and vibration control systems and robotics.